Mapping and Interpreting the Uppermost Mantle Reflectivity Beneath Central and South-West Iberia

I. Palomeras[1], P. Ayarza[1], J. Andrés[2], A. M. Álvarez-Valero[1], J. Gómez-Barreiro[1], J. Díaz[2], J. Alcalde[2], R. Carbonell[2]

[1] Department of Geology, University of Salamanca, Salamanca, Spain

[2] CSIC-GeoSciences Barcelona (Geo3BCN-CSIC), Lluis Sole i Sabaris s/n, 08028, Barcelona, Spain

Corresponding author: Imma Palomeras (imma@usal.es)

Key Points:

- Two uppermost mantle P-wave reflections observed beneath the SW-Iberian Peninsula at 50-75 (H) km and 90-110 (L) km depth.
- 'H' corresponds to an increase in velocity and is likely the Hales discontinuity. 'L' is related to velocity decrease at the LAB.
- Full-wavefield modeling shows the Hales discontinuity corresponds to a zone of randomly distributed thin bodies with small Vp variations.

This article has been accepted for publication and undergone full peer review but has not been through the copyediting, typesetting, pagination and proofreading process, which may lead to differences between this version and the Version of Record. Please cite this article as doi: 10.1029/2020JB019987.

Abstract

At least two sub-Moho reflectors have been identified in different seismic refraction and wide-angle reflection experiments conducted in western Iberia since the early 1990s. The wavelet kinematics and characteristics of the shallowest event are probably produced by an increase in P-wave velocity that forward modeling places at ~70-75 km depth beneath the Ossa-Morena Zone (OMZ) shallowing up to 50-60 km beneath the Central Iberian Zone (CIZ). Synthetic modeling suggests that the coda and amplitude of this arrival may correspond to a ~10-km-thick heterogeneous layer. We used a 2D second-order finite-difference acoustic full wave-field modeling scheme with an input model which includes a layer of randomly distributed bodies thinner than ¼ of the wavelength of the source waves and $\Delta Vp=\pm 0.1$ km/s at the considered depth range. The resulting synthetic data reproduce well the observed amplitudes and codas because of the constructive interferences caused by this heterogeneous zone. The origin of this layer also discussed here in detail, is very likely related to the phase transition from spinel to garnet lherzolite, the so-called Hales discontinuity. A second reflection also observed in some of the experiments suggests the presence of a velocity inversion at greater depths. Forward modeling places this discontinuity at around 90 km depth beneath the OMZ, deepening to 105-110 km depth beneath the southeast CIZ and shallowing up to 80 km depth in the northeast CIZ. The observed characteristics of this event are consistent with those of the lithosphere-asthenosphere boundary.

Plain Language Summary

The continental upper mantle is considered to be homogeneous, mainly composed of peridotite. However, compositional changes exist, and the seismic reflectivity observed with different seismic methods suggests the presence of certain localized layering within the lithospheric mantle. Western Iberia (Spain) has been sampled by multiple active source seismic surveys that illuminated the uppermost mantle, showing strong upper mantle reflections. The arrival time and nature of the shallowest among the upper mantle reflections indicate that it corresponds to a positive velocity contrast placed at ~50-75 km depth (depending on the tectonic zone). To reproduce the recorded characteristics of the signal we introduced a ~10 km thick heterogeneous layer in the velocity model consisting of randomly distributed thin bodies with small velocity variations at the considered depth. The characteristics of this layer (contrast in physical properties and depth) agree with those of the transition from spinel to garnet lherzolite, the so-called Hales discontinuity. The seismic datasets also recorded a second deeper reflection, whose origin can be attributed to a velocity decrease with depth at ~90-110 km depth. Due to its characteristics and observed depth, we interpreted this reflector as the lithosphere-asthenosphere boundary.

1 Introduction

Observations from field sampling (i.e. mantle xenoliths and outcrops of exhumed mantle) and indirect methods (e.g. the range of measured seismic velocities) suggest that the continental upper mantle is mainly peridotitic in composition. However, the mantle's composition is not uniform (e.g. *Stracke*, 2012), and the significant lithological and structural heterogeneities can produce impedance contrasts high enough to be observed in seismic data [*Fumagalli and Klemme*, 2015]. The birth and evolution of new seismic techniques and the densification of

seismic arrays have confirmed the presence of layering within the continental lithosphere, with numerous positive and negative velocity change at the discontinuities [e.g. *Thybo and Anderson*, 2006; *Clowes et al.*, 2010, and references therein].

Seismic reflections are related to variations in the physical properties of subsurface rocks due to compositional changes, phase transitions, strain state variations or anisotropy. All these scenarios are capable of producing upper mantle reflections and have been invoked by several authors to explain the observed reflectivity in the lithospheric mantle. One of such lithospheric reflectors is the Hales discontinuity, named after *Hales* [1969]. It was observed at ~60-90 km depth because of an increase in isotropic velocity. This sub-Moho positive seismic impedance ($z=V*\rho$, where z is the seismic impedance, V is the seismic wave velocity and ρ is the density) contrast is observed at different places around the globe by different means:, *e.g.*, long-range controlled source experiments [*Hales*, 1969; *Hales et al.*, 1980; *Massé*, 1987; *Hajnal et al.*, 1997; *Musacchio et al.*, 2004; *Ayarza et al.*, 2010], shear-coupled P-waves [*Zand and Randall*, 1985], ScS reverberations [*Revenaugh and Jordan*, 1991], precursors to sSH [*Zhang and Lay*, 1993], receiver functions [*Bostock*, 1998; *Levin and Park*, 2000; *Saul et al.*, 2000], joint inversion of Rayleigh wave and receiver functions [*Anand et al.*, 2017], and, most recently, autocorrelations of ambient seismic noise [*Taylor et al.*, 2016; *Andrés et al.*, 2020]. The origin of this upper mantle discontinuity has been attributed to (i) compositional changes related to the existence of eclogitized subducted oceanic crust [*Snyder*, 1991; *Chian et al.*, 1998; *Cook et al.*, 2004], (ii) petrological changes responding to a phase transition from spinel-garnet to garnet-only peridotites [*Hales*, 1969; *Fernández Viejo and Clowes*, 2003; *Ayarza et al.*, 2010; *Anand et al.*, 2017], and (iii) velocity anisotropy variations [*Fuchs*, 1983; *Bostock*, 1997, 1998; *Levin and Park*, 2000]. Also, the fact that this feature is observed by controlled source seismic profiles around the world, led some authors to suggest that a global discontinuity located at 80-100 km depth may exist [*Pavlenkova*, 1996; *Steer et al.*, 1998]. Although lithospheric discontinuities certainly exist, the worldwide presence of the Hales discontinuity has not been proven yet.

Since the early 1990s, the Iberian Massif in western Iberia (Figure 1) has been sampled by multiple active source seismic surveys. These experiments employed energy sources large enough to illuminate the uppermost mantle, and their results showed strong sub-Moho arrivals at large offsets (>180 km) that reflect off an interface which depth concurs with those assumed for the Hales discontinuity. The ILIHA-DSS experiment [*Iliha DSS Group*, 1993] sampled up to three different mantle reflectors in western Iberia, demarcating different azimuthal anisotropy [*Díaz et al.*, 1993]. The IBERSEIS-WA profiles in southwestern Iberia [*Palomeras et al.*, 2009] showed strong uppermost mantle arrivals interpreted as the spinel- to garnet-lherzolite phase transition [*Ayarza et al.*, 2010]. The ALCUDIA-WA and NI (wide-angle and normal incidence) seismic profiles, placed to the north of the IBERSEIS profiles, showed a number of subcrustal reflections, yet, un-interpreted. In this work, we study the uppermost mantle reflections imaged by all these experiments in order to produce a joint interpretation of this reflectivity. Furthermore, we use synthetic seismic modeling to explain the particular characteristics exhibited by these subcrustal features. The aim of this manuscript is hence to address the source of this upper mantle reflectivity, defining its extension and regional-scale relevance in relation to the Iberian Massif.

2 Geological Setting

The Iberian Massif is the largest outcrop of the Variscan belt in Western Europe (Figure 1). The latter resulted from the collision of the Laurussia and Gondwana continents during the late Paleozoic, resulting in the closure of the Rheic Ocean [*Martínez Catalán et al.*, 2007; *Azor et al.*, 2008, 2019]. During the convergence and collision, several allochtonous terranes were involved, defining a complex suture pattern along the orogen [*Gómez Barreiro et al.*, 2010; *Ballèvre et al.*, 2014; *Martínez Catalán et al.*, 2019; *Quesada et al.*, 2019]. Later on, a transpressional tectonic regime is inferred from the structure, variably modified by gravitational re-equilibration in the hinterland and by the formation of orogenic bends (oroclinals) [e.g. *Martínez Catalán*, 2012; *Azor et al.*, 2019].

The north and southwest branches of the Iberian Massif are conventionally divided in different tectonostratigraphic zones, from hinterland to foreland: a) the north branch includes the Galicia-Trás-os-Montes Zone (GTMZ), the Central Iberian Zone (CIZ), the West-Asturian Leonese Zone (WALZ) and the Cantabrian Zone (CZ); b) the southwest branch includes the southern part of the CIZ, the Ossa-Morena Zone (OMZ) and the South Portuguese Zone (SPZ) (Figure 1). Focusing on the southwest branch of the Iberian Massif, the CIZ formed part of the passive margin of Gondwana, whereas the OMZ was probably a continental terrain that had partly drifted away from Gondwana [*Fonseca and Ribeiro*, 1993; *Azor et al.*, 2008].

Tectonic processes were diachronous across the belt and included several phases. In the southwestern branch, an initial compression occurred during Devonian times (390-360 Ma) and related to subduction/collision affected the OMZ and the southern boundary of the CIZ [*Simancas et al.*, 2003]. In the Mississippian (360-330 Ma), an extensional episode affected the SPZ, OMZ, and southernmost CIZ, producing, normal faulting, basin filling, gneissic domes, and mafic magmatism [*Dias da Silva et al.*, 2018]. A second compressional episode developed in the Late Mississippian-Early Pennsylvanian (330-310 Ma) times, and recorded in SPZ and OMZ, resulted in an inversion of basins and upright folding. A late extensional episode is observed during the late Pennsylvanian-Permian (310-280 Ma), producing normal faulting and some late-orogenic granitic magmatism. Transcurrent deformation, both transpression and transtension, was important during the orogeny as clearly demonstrated by the development of large wrench shear zones formed at late orogenic episodes [e.g. *Silva and Pereira*, 2004; *Martinez Catalan*, 2011].

The western Iberian massif has been largely stable since the end of the Permian, and Paleozoic basement rocks are exposed in the area. Crustal thickness averages 31-32 km, in the southern CIZ, OMZ, and SPZ, deepening to 35 km near the Central System [*Diaz et al.*, 2016; *Palomeras et al.*, 2017] the latter being probably the result of Alpine reworking [*Ehsan et al.*, 2015; *Andrés et al.*, 2019].

3 Controlled Source Seismic Surveys sampling the Uppermost Mantle of SW Iberia

Three seismic experiments have sampled the crust and uppermost mantle in the southwestern and western part of the Iberian Massif (Figure 1 and table 1): the ILIHA-DSS, the IBERSEIS, and the ALCUDIA experiments. The ILIHA-DSS consisted in a set of wide-angle profiles across the Iberian Peninsula, whereas both the IBERSEIS and ALCUDIA experiments consisted in

coincident wide-angle and normal incidence surveys, acquired across the south and center of the Iberian Massif respectively (Figure 1).

3.1. ILIHA-DSS experiment

The ILIHA-DSS experiment, acquired in the early 1990s [*Iliha DSS Group*, 1993], was a large deep seismic sounding experiment designed to study the uppermost mantle (from 30 to ~100 km depth) of the entire Iberian Massif. It consisted of a set of six wide-angle transects across the Iberian Peninsula, with station spacing of 5-10 km on average. The source employed consisted of 500 to 1000 kg of explosives fired offshore at the edges of the profiles. In this paper, we focus on the four transects that cross through the study area: Line BX, Line DA, Line BE, and Line CF (Figure 1). These transects, three of them reversed and one unreversed, present offsets larger than 600 km and sample the Iberian Massif lithosphere at different azimuths. The ILIHA-DSS analysis indicated the presence of 3 sub-Moho reflectors beneath southwest Iberia [*Iliha DSS Group*, 1993] at 45, 68, and 88 km depth portraying a layered mantle lithosphere with differentiated P-wave velocity and azimuthal anisotropy [*Díaz et al.*, 1993].

3.2. IBERSEIS experiment

In the 2000s, the IBERSEIS project was launched with the aim of acquiring high-resolution seismic data in the lithosphere of southwest Iberia. One normal incidence (NI) and two wide-angle (WA) profiles were acquired between 2001 and 2003. The IBERSEIS-NI was a ~300 km long normal incidence reflection experiment (table 1) that crossed, from south to north, the SPZ, the OMZ, the CIZ, and their respective sutures, providing a detailed crustal image [*Simancas et al.*, 2003]. The profile exhibited a reflective crust with a clear reflection at its base, but a seismically transparent mantle [*Simancas et al.*, 2003; *Ayarza et al.*, 2010]. To further investigate the nature of the lithosphere , two wide-angle reflection/refraction transects (IBERSEIS-WA) (table 1) were also acquired [*Palomeras et al.*, 2009]. Transect A overlapped the IBERSEIS-NI section and Transect B sat west from Transect A, sharing its northern edge (Figure 1). In contrast to what the IBERSEIS-NI results show, both transects present clear sub-Moho reflections at large offsets (>180 km): *e.g.*, in shots 2 and 3 on Transect A, and shots 1 and 6 on Transect B [*Ayarza et al.*, 2010]. These reflections were first interpreted as an interface at 65-70 km depth featuring a Vp contrast from 8.3 km/s to 8.5 Km/s [*Palomeras et al.*, 2009]. A later detailed analysis of this phase [*Ayarza et al.*, 2010] found that to reproduce the observed high amplitudes and arrival times, it must reflect off a ~10 km thick band located at ~60-70 km depth, containing ~150 m wide heterogeneities and being characterized by a velocity increase from 8.2 to 8.3 km/s. These attributes are aligned with the overall characteristics predicted for the spinel- to garnet-lherzolite phase transition, the so-called Hales discontinuity. As stated above, despite strong reflections from the mantle are observed in the IBERSEIS wide-angle reflection/refraction surveys, no upper mantle reflectivity is identified in the IBERSEIS-NI transect. *Ayarza et al.* [2010] outlined four possible reasons that might explain this contrasting seismic signature in both coincident datasets: 1) the impedance contrast of this interface is not strong enough and needs a tuning effect not met with the vertical incidence seismic frequencies; 2) the reflection coefficients at low incidence angles are lower than at wide-angle higher incidence angles; 3) vertical incidence data is less sensitive to gradient zones such as the modeled Hales discontinuity; and/or 4) mid-point projections of both data sets do not exactly coincide and thus, they might not be sampling the same exact area.

3.4. ALCUDIA experiment

The ALCUDIA experiments were designed to image the CIZ to the northeast of the previous IBERSEIS profiles. The ALCUDIA project also included two seismic experiments: 1) the ALCUDIA-NI, a ~250 km-long normal incidence profile across the CIZ [*Martínez Poyatos et al.*, 2012], and 2) the ALCUDIA-WA, a ~300 km long wide-angle reflection/refraction profile that overlaps the ALCUDIA-NI [*Ehsan et al.*, 2015] (Figure 1, Table 1)

The ALCUDIA-NI is a high-resolution normal incidence profile [*Martínez Poyatos et al.* 2012] which provides a detailed image of the crust with a clear Moho discontinuity at 10 s two-way travel time (twtt), c. ~30km depth. Contrary to the IBERSEIS-NI section and despite having exactly the same acquisition parameters, the ALCUDIA-NI imaged ~20 km-long sub-horizontal continuous strong reflectors at ~14-17 and ~18-20 s twtt in the northern and central part of the profile, beneath common depth points (CDP) ~1200 to ~2000 and ~6000 to ~7200 respectively [*Martínez Poyatos et al.*, 2012] (Figure 2). Assuming a crustal velocity of 6 km/s and a mantle velocity of 8.0 km/s [*Ehsan et al.*, 2015], these reflectors correspond to an interface at 54 km depth to the north, below CDP 1000-2000, and at 66 km depth at the center, below CDP 6200-7000. However, there is no interpretation to date for these features. The design of the ALCUDIA-WA profile mimics that of the IBERSEIS-WA (Table 1) [*Ehsan et al.*, 2015] and was aimed to provide the P-wave velocity distribution of the lithosphere in the CIZ. The large offsets of shot gather 1, 4, and 5 allow the identification of deep arrivals indicating the presence of sub-Moho reflectors in the region. These reflections are, as yet, un-interpreted and only crustal models have been published up to date. In this work, we model these reflections.

4. Modeling of the uppermost mantle reflections

4.1. ALCUDIA-WA: Modeling of the uppermost mantle

The ALCUDIA-WA crustal phases have been already interpreted [*Ehsan et al.*, 2015], providing a detailed model limited to the crust. This work focuses on the modeling of the observed uppermost mantle arrivals. In this study we also present shot gather 1, which was not included in the crustal modeling presented in *Ehsan et al.* [2015]. In addition, we also tested different processing flows and parameters to improve the coherency of the signal and to facilitate identification of different phases reflecting off the upper mantle. Picked arrivals will be labeled as follows: Pn for the head wave traveling within the upper mantle, PmP for the P-wave reflected at the base of the crust (Moho), and PM_iP for the upper mantle reflected phases, where *i* represents the phase (i.e. 1 or 2).

Several upper mantle reflections are observed in shot gathers 1, 4, and 5 of the ALCUDIA-WA profile (Figure 3). A strong arrival is seen in shot 1 at large offsets (from190 km to the end of the line) and ~7 s (hereafter, reduced time, reduction velocity=8 km/s). It features higher amplitudes than Pn and can be followed up to 250 km offsets. This arrival presents a conspicuous coda of ~1 s (Figure 3, PM_1P phase) that mimics the one observed in the IBERSEIS-WA shot gathers at similar offsets and times [*Ayarza et al.*, 2010]. Shot 4 presents an arrival at ~190 km to 210 km offset and 10 s that extends along ~25 km with very high amplitudes. This phase has similar characteristics to the PM_1P phase on shot 1, with similar ~1s-long coda and it has been labeled as

PM_1P in Figure 3 as well. Another set of deeper discontinuous reflections is observed in shots 4 and 5 at offsets greater than 150 km until the farther offsets and between 13 and 14 s twtt (Figure 3, PM_2P).

To understand these subcrustal arrivals, we first tested if they could correspond to a P-to-S wave conversion at the Moho discontinuity (i.e. the PmS phase) or vice versa (i.e. the SmP phase). For a 30 km-thick crust with average P- and S-wave velocities of 6 and 3.6 km/s respectively, the PmS/SmP phase would arrive at 46.40 s twtt at 200 km offset, or 21.40 s at a reduced velocity of 8 km/s. The sub-Moho arrivals that are under study arrive much earlier than these theoretical times, thus rejecting the hypothesis that they correspond to converted waves.

We carried out a spectral analysis in order to better study the attributes of these phases. The dominant frequency of the PM_1P phase is in the range of 7-10 Hz (Figure 4a and 4b), whereas the PM_2P phase, has its highest amplitudes at a lower frequency range (< 10 Hz, Figure 4c and 4d). According to these results, a bandpass filter of 5-20 Hz was applied to the data with the goal to enhance the image of both phases.

A further analysis step focused on the polarity of the phases, which provides information about the impedance contrast (positive or negative) of the interfaces that generate the reflections. We compared the polarity of subcrustal reflections with that of the PmP phase, whose polarity responds to an impulsive source reflected off a positive impedance contrast (crust to mantle). Accordingly, we stacked traces that encompass both reflections and compared the resulting wiggle with the one obtained from stacking PmP arrivals (Figure 5). Stacking of PM_1P arrivals of shots 1 and 4 results in a reflection with the same positive polarity as the PmP arrival, indicating that the PM_1P phase most likely reflects off an interface that features an increase in seismic impedance (Vp and density) with depth. On the other hand, the stack of deeper PM_2P reflections observed in shots 4 and 5 into single traces shows that their polarity is negative, the opposite to that observed in the PmP.

Once the above-mentioned reflections were attributed to contrasting impedance variations, mantle reflections were modeled using the ray-tracing based utilities developed by *Zelt and Smith* [1992], taking into account that the crustal structure of the area sampled by the ALCUDIA experiment is well constrained [*Martínez Poyatos et al.*, 2012; *Ehsan et al.*, 2014, 2015]. The work presented in this manuscript extends the crustal velocity model of *Ehsan et al.* [2015] into the upper mantle resulting in a 2D P-wave velocity structure down to 120 km depth (Figure 6).

The sub-Moho Vp velocity is constrained by the Pn phase at 8.0-8.15 km/s [*Ehsan et al.*, 2015]. From there, we modeled a gradual increase of Vp with depth. As no direct nor head waves coming from the upper mantle interfaces are recorded, both the velocities and depths of the reflectors are constrained by the reflected wave. Therefore, to model these interfaces we must assume a tradeoff between velocity and depth of the reflector. The Earth velocity models (IASP91 and AK135 1D Earth velocity-depth models [*Kennett and Engdahl*, 1991; *Kennett et al.*, 1995]) and petrological analysis in xenoliths establish that the lithospheric mantle velocities range between 7.9 to 8.4 km/s. So, we restricted the possible mantle velocities to this range of velocities and varied both velocity and depth of the interface to adjust the arrival times. As a result, the positive polarity of the PM_1P phase is considered to be related to an increase in Vp from 8.2 to 8.3 km/s at around ~ 51 km depth to the south of the ALCUDIA-WA section deepening to 57 km depth to the north. On the other hand, the PM_2P phase, which presents inverse polarity when compared with PmP, corresponds to a decrease in Vp from 8.3 to 8.0 km/s

on an interface located at 100 km depth that sinks to 113 km depth to the north (Figure 6). Although some of the observed reflections are not continuous enough to be considered profile-long structures, they have been modeled as such for computational reasons. We will discuss the nature of these reflectors in the following sections.

The lateral resolution of the interfaces is constrained by the length of the identified phases and by those areas sampled by rays. Raytracing in Figure 6 indicates the range of distances in which each interface is sampled. Figure 6 also shows the agreement of the calculated travel times with the energy recorded in every shot record. The derived P wave velocity model reproduces the picked travel time branches with a very good agreement (< 0.1 s) with a maximum difference between the calculated and observed arrival times of 0.2 s for PM_2P on shot A4. The model uncertainties are given by the maximum alteration of the depth of the interfaces and the upper mantle velocity that still retains the fit to the observed travel times. The estimated uncertainty on depth is ±1 km and ±3 km for PM_1P and PM_2P, respectively. For the P-wave velocities, the uncertainty is of 0.15 km/s.

4.2. ILIHA-DSS Modeling

In this paper, the P-wave velocity models from the ILIHA-DSS experiment [*Iliha DSS Group*, 1993] are reevaluated in the light of the new high-resolution IBERSEIS-WA and ALCUDIA-WA data and crustal models. Previous lithospheric models interpreted up to three high amplitude subcrustal phases as alternating thin (<5 km) low- and high-velocity layers in the uppermost mantle. This layered geometry was necessary to produce an impedance contrast high enough to reproduce the observed amplitudes. When such low-velocity layers (7.7 km/s) are included in the model, the underlying high velocities need to reach up to 8.6 km/s in order to fit both amplitudes and travel times. However, such high velocities are not expected at depths shallower than ~300 km according to the IASP91 and AK135 1D Earth velocity-depth models [*Kennett and Engdahl*, 1991; *Kennett et al.*, 1995]. Furthermore, studies on the estimation of lithospheric mantle properties based on the petrological analysis in xenoliths indicate that at 100 km depth, P-wave velocity beneath tectons (areas where the crust was formed or modified not later than 1Ga) is in the range of 8.20-8.25 km/s [*Griffin et al.*, 2009]. In order to reconcile the observed phases and the models with the estimated velocity from these petrological studies, we have tried to adjust the observed ILIHA experiment travel times with lower (< 8.4 km/s) P-wave velocities. Following this strategy, we have performed forward modeling using the same code [*Zelt and Smith*, 1992] to obtain the velocity distribution along the four transects presented here: lines BX, DA, BE, and CF (Figures 1 and 7). The crustal part of the models is based on the results of the IBERSEIS-WA and the ALCUDIA-WA experiments when sampling the same tectonic zones, thus allowing a well-constrained velocity and structure at that level. Similarly, to the IBERSEIS-WA and ALCUDIA-WA datasets, we assumed that the shallowest arrival (PM_1P) is produced by a positive impedance contrast (P-wave velocity increases from 8.2 km/s to 8.3 km/s). For a closer inspection of the identified phases, the reader is referred to *Iliha DSS Group* [1993]

4.2.1. Line DA

Line DA is an unreversed ~720 km-long line, hence only shot D1 is analyzed (Figures 1 and 7a). Two phases were picked by the *Iliha DSS Group* [1993]. A first clear arrival appears at 230-400 km offset and 8.0 s twtt. This phase has a wave coda of ~1 s twtt. A second arrival is

identified at 390 km offset and 8 s twtt. Forward raytracing modeling indicates that the first arrival (PM_1P) corresponds to a reflector placed at 75 km depth beneath the OMZ (Figure 7a). The second arrival is modeled as an interface at 90 km depth beneath the OMZ-CIZ with a P-wave velocity decrease from 8.3 to 8.0 km/s.

4.2.2. Line BX

Two shots were fired for reversed line BX, one at each edge of the ~680 km-long profile (Figures 1 and 7b). Three separated arrivals were picked for shot B2 [*Iliha DSS Group*, 1993]. The shallowest one (PM_1P) is observed from 240 to 390 km offset and 6.5 s twtt. A second arrival is identified at 350 km offsets and 7 s twtt. A later arrival is picked at 420 km offset and 7.5 s (PM_2P). On the other edge, shot X2 presents also three upper mantle arrivals: at ~7 s and offsets of 200 km (PM_1P), at 8 s and 280 km offset, and at 8 s twtt and 440 km offset (PM_2P). The shallowest arrivals have thus been modeled as a reflector at 62 km depth to the north (beneath the western part of the CIZ) that shallows up to 60 km to the south (beneath the OMZ and the Guadalquivir basin). The second interface is modeled as reflected from an interface at 72 km depth beneath the western part of the CIZ and 84 km depth beneath the OMZ. The deepest interface is modeled to adjust the later arrivals from shots B2 and X2. These match the travel time of reflections off an interface placed at 95-100 km depth featuring a decrease in velocity from 8.3 to 8.0 km/s (Figure 7b).

4.2.3. Line CF

This reversed ~1220 km-long line presents two upper mantle arrivals on shot C [*Iliha DSS Group*, 1993]. A strong arrival is observed at ~270 km offset and ~7 s twtt (PM_1P). As in the other lines, this sub-Moho arrival has a ~1s length wave coda. Forward modeling indicates that this arrival originates at an interface at 72 km depth beneath the OMZ (Figure 7c). A second arrival is observed at 440 km offset and 7.5 s twtt (PM_2P). This phase is modeled as a reflection coming up from an interface placed at 90 km depth beneath the CIZ (Figure 7c). In agreement with line BX, a decrease in velocity with depth from 8.3 to 8.0 km/s is proposed.

4.2.4. Line BE

This line extends for more than 900 km from west to east across the Iberian Peninsula (Figures 1 and 7d). Shot B1 recorded two sub-Moho arrivals [*Iliha DSS Group*, 1993]. A shallow arrival is identified at 200 km offset and 6.5 s twtt (PM_1P). This interface is modeled at 55 km depth beneath the northern part of the CIZ. A second arrival observed at 380 km offset and 7 s twtt is modeled as reflected from an interface placed at 80 km depth beneath the same area of the CIZ (Figure 7d). Again, it corresponds to a decrease in the P-wave velocity with depth.

The new velocity models obtained from the ILIHA dataset do not require the existence of high- and low-velocity zones to fit the observed arrivals. Instead, a more reasonable gradient velocity zone with velocities ranging from 8.2 to 8.3 km/s and a negative velocity contrast between 8.3km/s and 8.0 km/s can reproduce the observed travel times. Even though, in this case, we cannot investigate the polarity of reflections, the modeling results indicate that these come from interfaces located at similar origins to those imaged in the IBERSEIS-WA and ALCUDIA-WA

and that therefore represent the same features. Our new models (Figure 7) locate the three upper mantle discontinuities slightly deeper than in previous velocity models [*Iliha DSS Group*, 1993].

5. Characteristics of the SW-Iberia Sub-Moho Subcritical Reflection, PM_1P

We have observed the shallowest reflector PM_1P along three different wide-angle reflection surveys. The resulting velocity models fit its travel time at all the surveys, but a simple layer cake model cannot reproduce the high amplitude and ~1s coda observed in all shot gathers for this phase. In this section, we discuss in detail the nature and potential origin of this fabric.

The shallowest upper mantle reflector appears to exist below the OMZ and CIZ in the wide depth range of 50-75 km. This boundary produces reflections at large offsets and it is observed discontinuously as a few tens of kilometers sub-horizontal feature. In addition, a similar reflective pattern is observed in the ALCUDIA-NI (normal-incidence) profile, where ~20 km long mantle reflections are imaged between ~16 and ~19 s twtt (Figure 2). Recent seismic transect in northwest and central Iberia [*Andrés et al.*, 2019] have imaged the upper mantle reflectors beneath the Duero Basin and the Central System at similar depths: 12-13 s and 15 s twtt for the shallowest reflector, and 18 s twtt for the deepest. As these reflections are not continuous in any of the studied datasets, we cannot state that they represent a single, orogen-scale interface extending below the entire CIZ and OMZ. However, some considerations should be made regarding this point.

The Fresnel zone contributes to the formation of the reflected wave fields determining the minimum size of a structure that can be resolved. The size of the Fresnel zone, and hence the lateral seismic resolution, is strongly dependent on the dominant frequency and depth. Vertical resolution is determined by ¼ of the dominant wavelength ($\lambda/4$). The datasets presented in this study have a dominant frequency of around 8 Hz for the PM_1P phase, which implies a lateral and vertical resolution of 5-5.5 km and ~250 m, respectively, at depths of 60 km. Moreover, *Andrés et al.* [2020], use dominant frequencies of 4 Hz in their ambient noise autocorrelation study, which implies Fresnel zones of around 7.8 km at the same depth. This indicates that subsurface zones smaller than these values cannot be individualized or even detected by the experiments presented here, establishing a minimum lateral extent for the modeled feature. Accordingly, two possibilities exist for the geometry of this reflector: (i) it is characterized by sets of a few km-long (15-20 km) flat features distributed heterogeneously below the OMZ and CIZ at 50-75 km depth range; or (ii) it is a more or less laterally continuous gradient zone with variable characteristics that result in a layered pattern that produces discontinuous reflectivity depending on incidence angles, wavelengths and, accordingly, development of reverberating mechanisms. It is noteworthy that although high-angle reflections are expected in wide-angle experiments, the phases analyzed here correspond to sub-critical reflections. At these angles, reflection coefficients are higher than at vertical incidence but lower than those at critical and supercritical angles [*Aki and Richards*, 2002] and therefore, less energy is reflected off the interfaces, making such features difficult to observe.

The sub-Moho reflections in the ALCUDIA-WA (Figure 3), IBERSEIS-WA and the ILIHA-DSS (Figure 7) shot records show a distinctive high amplitude, ~1 s long, coherent coda. Multiple similar sub-Moho reflections with a complex coda have been recorded around the world

[e.g. *Morozov et al.*, 1998; *Nielsen et al.*, 2003; *Carbonell*, 2004; references in *Clowes et al.*, 2010]. The signal characteristics of these arrivals have been linked to two potential causes: (i) these are multiples of refractions and reflections within the uppermost mantle produced by the Moho and free-surfaces [*Morozov et al.*, 1998; *Morozov and Smithson*, 2000]. These authors interpreted the long coda of the teleseismic Pn phase that is observed at offsets larger than 2000 km as a sub-Moho 'whispering-gallery wave' [e.g. *Chapman*, 2004] traveling within the uppermost mantle. However, neither the phase (Pn), arrival times nor the offsets observed in the SW Iberia wide-angle reflection/refraction data agree with these observed by the authors. (ii) Multiple reflections and scattering within a heterogeneous upper mantle [*Thybo and Perchuc*, 1997; *Fuchs et al.*, 2002; *Carbonell*, 2004; *Ayarza et al.*, 2010]. These authors interpret reverberations by randomly distributed heterogeneous bodies with velocity fluctuations in the range of 1-2 %. The size of these heterogeneities is in the range of 20-40 km long and 0.15-2 km thick, depending on the authors. In some cases, a fabric of 1-2 km thick heterogeneities, with a small velocity contrast (<±0.1 km/s) needed to be included to reproduce the observed coda [*Hammer and Clowes*, 2004]. *Ayarza et al.* [2010] already proved that the signal observed in the IBERSEIS-WA shot gathers could be reproduced by a ~10 km thick heterogeneous gradient zone located at ~ 60 km depth, with a total velocity contrast of 1.3%, from 8.2 to 8.3 km/s. The size of the random heterogeneities had to be around 150 m thick in order to produce constructive interferences at the dominant frequency of their dataset to reproduce the offset, time, amplitudes and the ~1 s thick coda. Since the ILIHA-DSS and ALCUDIA-WA sample the same area and the shallowest subcrustal arrivals show the same characteristics than these observed in the IBERSEIS-WA dataset, we suggest that a stochastic distribution of elliptical/elongated bodies is the likely cause of the SW-Iberia lower lithosphere reflections. As the velocity contrast from 8.2 to 8.3 km/s is not high enough to produce the high amplitude of the observed reflections, constructive interferences are needed to achieve phases with the observed amplitudes, higher than those of Pn in some shot gathers (Figure 3). Thus, a band of heterogeneities around 150-200 m in thickness extending from 55 km to 85 km depth with a velocity contrast of less than 1% may be a realistic model. When the thickness of the layering differs from the one proposed here, the reflector is simply not visible to our datasets, thus appearing as a discontinuous feature. This hypothesis is tested in next section.

6. Synthetic Modeling of PM_1P and PM_2P

The 2-D P-wave velocity model for the uppermost mantle is based on a forward approach, which uses simple layer cake models and a relatively simple parameterization for velocity and boundary nodes. Hence, models in Figures 6 and 7 represent an averaged P-wave velocity distribution that fits the picked travel times but does not take into account the reflectivity (Figure S1). In order to reproduce the observed complexity of the PM_1P reflection, the modeling needs to consider the full propagation of an acoustic P-wave. To that end, we have built a ~420 km-long reference P-wave velocity model for the southern Iberian lithosphere. We use the P-wave velocity distribution of the IBERSEIS-WA for the SPZ and OMZ, and the ALCUDIA-WA results for the CIZ. Two ~15 and ~2 km thick heterogeneity zones are included, one at the depth of occurrence of the PM_1P reflection and the other at the base of the crust, respectively (Figure 9b). Within these bands, velocity fluctuations in the range ±0.1 km/s are randomly distributed following a 2.7 fractal dimension [*Holliger and Levander*, 1992] (Figure 9b). This self-similar bimodal velocity distribution is considered to be a good approximation to the structural

complexity of the lower crust and upper mantle observed in exposed cross-sections [*Girardeau et al.*, 1989; *Holliger and Levander*, 1992]. The horizontal and vertical correlation length of the heterogeneities are 3 km and 250 m respectively.

Five synthetic shot gathers were calculated using a 2D second-order explicit finite-difference scheme [*Zahradník et al.*, 1994] with absorbing boundary conditions at the sides and bottom of the model [*Sochacki et al.*, 1987]. The calculated shots gathers are distributed along the line coincident with the position of the IBERSEIS-WA and ALCUDIA-WA shots that recorded the uppermost mantle reflections: one at each edge of the profile (shots A and E) and three along the line at km 150 (shot B), 212 (shot C), and 353 (shot D) (Figure 9d). We used a minimum phase Ricker wavelet with a dominant frequency of 8 Hz to simulate the energy source since that is the dominant frequency content of the upper mantle reflection. The resulting shot gathers, with a trace spacing of 300 m, are presented in Figure 9d. The primary phases (Pg, PmP, Pn, PM_1P, PM_2P) are clearly recognizable, and have been labeled accordingly. Next, we will focus on the description of PM_1P and PM_2P phases that are the focus of this study.

- Synthetic shot A (Figure 9d) corresponds to shot 6 of the IBERSEIS-WA Transect B [*Ayarza et al.*, 2010] (Figure 9c). The Moho discontinuity is clearly imaged, including a good recovery of the high amplitudes observed in the field data. The prominent PM_1P phase observed in the IBERSEIS-WA shot at ~193 km offset and 8.0 s (velocity of reduction of 8.0 km/s) is reproduced on the synthetic shot A with the ~1 s coda, although it features a slightly lower amplitude. Synthetic shot A also presents a clear PM_2P phase at ~13 s and 190 km offsets.
- Synthetic shot B corresponds to the ALCUDIA-WA shot 1 (Figure 9c). Shot B presents a clear Pn phase and the base of the crust reflection (PmP phase), both observed in the field data but with lower amplitudes. The PM_1P phase is reproduced regarding travel time and offsets, although with lesser energy than the observed in the field data.
- Synthetic shot C corresponds to shot gather 1 of the IBERSEIS-WA Transect B (Figure 9). This synthetic shot presents a higher energy Pn phase than that observed in the field data. On the other side, the synthetic PmP phase reproduces well the arrival time, amplitudes, and thickness of the reflective package observed in the field data. Like in previous shots, the PM_1P phase mimics the one observed in shot 1 (IBERSEIS Transect B) in arrival time, offset, and coda, but with lesser energy. The PM_2P phase observed in the synthetic shot C, at ~13 s at 200 km offsets, is also observed in the IBERSEIS-WA shot. This phase was not identified, interpreted, nor modeled in previous studies.
- Shot D corresponds to shot 4 of the ALCUDIA-WA transect (Figure 9). Its prominent PM_1P phase is not clearly observed in the synthetic. However, the PM_2P is clearly visible on the synthetic shot at the expected travel time and offsets. This phase is only visible at large offsets on the field data. This pattern is also reproduced by the synthetic shot where the energy reflected from the base of the lithosphere increases with offset (larger incidence angles and thus, larger reflection coefficients).
- Finally, synthetic shot E emulates the ALCUDIA-WA shot 5 (Figure 9). The reflection (PmP) and refraction (Pn) from the Moho discontinuity recover the arrival time, amplitudes and coda observed on the field shot gather. The weak PM_1P arrival observed in shot 5 is also reproduced on the synthetic shot. In the same way, the prominent PM_2P phase observed at ~13 s and -270 km offset is identified at the same time and offset on the

synthetic shot E. Again, the synthetic and real shot gathers present increasing energy/amplitude at larger offsets for this phase.

As a summary, the Moho discontinuity is clearly imaged in the five shot-gathers, reproducing the PmP phase recorded on the field data. The synthetic shots also reproduce the observed characteristics of the uppermost mantle recorded phases, where the amplitude levels are achieved by constructive interferences. These observations support our model of a gradient zone with heterogeneities extending from 70 to 85 km depth beneath the SPZ and OMZ and from 55 to 70 km depth beneath the CIZ as source of PM_1P. The total velocity contrast of this gradient zone is less than 1%.

7. Discussion

7.1. The south-west Iberia uppermost mantle reflector

Three wide-angle experiments recorded from the 1990s to 2012 imaged at least two sub-Moho reflectors in the southern and western part of the Iberian Massif. The shallowest reflector (PM_1P) has been modeled as a sub-horizontal gradient zone where velocities increase from 8.2 to 8.3 km/s with depth. The top of this gradient zone appears at different depths beneath each of the tectonic zones (Figure 8). It is placed at ~58 km depth beneath the OMZ-SPZ junction, around the Guadalquivir Basin (GB) (see ILIHA line BX, Figure 7b), whereas in the northern and central parts of the OMZ it is in the range of 67.5 to 75 km depth. Beneath the CIZ, the shallowest reflector rises to 50-62 km depth towards the north and east. The normal incidence profile ALCUDIA [*Martínez Poyatos et al.*, 2012] also images a set of sub-Moho reflections at ~18-20 s twtt at CDP 6000 to 7200 (km 100 to 130) and at ~14-17 s twtt at CDP 1200 to 2000 (km 10 to 40) (Figure 2). These reflections correspond to depths of 66 to 70 km and 46 to 58 km depth respectively, assuming an average Vp of 6 km/s for the crust and 8 km/s for the lithospheric mantle.

Since the late ’80s, numerous upper mantle reflectors have been reported from normal incidence profiles worldwide [*Steer et al.*, 1998 and references therein]. Different hypotheses have been invoked to explain their reflectivity: e.g. remnants of subducted oceanic lithosphere [*Warner et al.*, 1996; *Balling*, 2000; *Hansen and Balling*, 2004; *Clowes et al.*, 2010], deformation fabric related to subduction [*Alsdorf et al.*, 1996; *Abramovitz et al.*, 1998], occurrence of fluids, and mafic layering [*Warner and McGeary*, 1987]. Next, we are going to consider how these interpretations match our data.

Normal-incident sections that image old subduction zones usually show dipping upper mantle reflections which meet the crust-mantle boundary in a thickened crust with a marked Moho topography and Moho offset [*BABEL Working Group*, 1990; *Snyder and Flack*, 1990; *MONA LISA Working Group*, 1997; *Chian et al.*, 1998; *Cook et al.*, 1999; *Gorman et al.*, 2002]. A south-dipping reflection is observed in the ALCUDIA-NI seismic image just below the Moho on CDP 10000-11000 (Figure 2) but it does not comprise a significantly irregular Moho topography or a thickened crust. This featured crust-mantle wedge has been interpreted as a crocodile-like structure [*Meissner*, 1989] that accounts for ~30 km shortening at a lower crust level [*Martínez Poyatos et al.*, 2012], probably imaging an imbrication of different tectonic zones during the Variscan orogeny. That, together with the limited lateral extent and dip of this reflection and the existence of late tectonic transpression in the area preclude a direct correlation with the sub-horizontal and heterogeneous reflector modeled from our wide-angle data. In addition, the length

of the modeled feature (PM_1P source) exceeds that of the shortening in this area during the Variscan orogeny, thus hindering any relation with a Variscan subduction-related event.

It is widely accepted that shear zones and faults can generate seismic reflectivity [e.g. *Fountain et al.*, 1984; *Vissers et al.*, 1991, 1995; *Calvert*, 2004; *Zucali et al.*, 2014; *Gómez Barreiro et al.*, 2015; *Gomez Barreiro et al.*, 2018]. Accordingly, compressional and extensional events occurring in the area from the Devonian to the Late Carboniferous or even Permian (depending on the area), and affecting the crust, may have left an imprint at upper mantle level. In collisional contexts, geodynamic modeling typically shows that the strain localization produces ~45° dipping almost linear shear bands [*Frederiksen and Braun*, 2001]. However different and more complex geometries could appear when orogenic gravitational collapse and transpressive tectonics postdate deformation [e.g. *Azor et al.*, 2019]. Again, wide-angle modeling and normal incidence images for SW-Iberia do not show significant upper-mantle dipping reflectors. In addition, seismic images acquired in western Iberia do not show any tectonic feature offsetting the Moho, *i.e.* the crust-mantle boundary seems to have acted as a rheological discontinuity. Furthermore, observations of shear zones on exposed mantle rocks indicate changes in the petrophysical properties (mylonitization) [e.g. *Vissers et al.*, 1995; *Gómez Barreiro et al.*, 2015; *Gomez Barreiro et al.*, 2018] that lead to a reduction in the P-wave velocity. Synthetic shot gathers for a random shear zone in the uppermost mantle with 50% normal peridotites and 50% material with reduced Vp [*Hansen and Balling*, 2004] do not produce scattered waves. Our analysis indicates that the observed sub-Moho reflection PM_1P corresponds to a sub-horizontal reflector, featuring an increase in P-wave velocity with depth, and located at different levels, quite the opposite from what corresponds to a shear zone.

The existence of fluids is another likely source of mantle reflectivity as their zero shear modulus, can also produce an impedance contrast large enough to cause reflectivity [*Van Avendonk et al.*, 2011]. Fluids are likely to be present in young tectonic systems, i.e., subduction zones where water is introduced into the upper mantle along the upper part of the subducting slab via dehydration, and/or melt is produced along the subducted slab. This is not the case in the study area, where nowadays there are no active subduction processes. Thus, if fluids were present in the mantle in the past, they might have migrated or have been involved in mineral reactions. Another source of fluids could be the nearby Calatrava Volcanic Field (Figure 1, ~N39°/W°), a Neogene volcanic field that extends over 5000 km^2 on the southeast edge of the CIZ (Figure 1). Surface wave tomography studies indicate that partial melting exists underneath this field at shallow depths (65 km) [*Palomeras et al.*, 2014]. Although the presence of these magmas seems obvious, it is unlikely that they may inflow the lithospheric mantle of a wide area such as southwest and west Iberia (Figure 8). Therefore, we consider that the presence of fluids can be ruled out as the source of the southwest Iberia upper mantle reflectivity.

Finally, another potential source for the target reflectivity is the presence of mafic bodies partially transformed into eclogites [e.g. *Hansen and Balling*, 2004]. Depending on the availability of water and the rock composition, mafic rocks begin to transform into eclogites at about 35 km depth [*Green and Ringwood*, 1967a; *Ito and Kennedy*, 1971; *Hacker*, 1996]. The eclogite/peridotite seismic contrast could result in visible reflectivity [*Chian et al.*, 1998; *Wang et al.*, 2009; *Clowes et al.*, 2010; *Worthington et al.*, 2013]. However, a sub-horizontal layer of mafic rocks in the mantle could have a reflection coefficient large enough to be observed in vertical incidence seismic data as a continuous bright feature, something not seen here. But field observations suggest that eclogitization could be erratic, and small bodies are commonly

interbedded in peridotitic massifs [e.g. *Austrheim et al.*, 1997; *Medaris et al.*, 2018]. We will discuss this hypothesis in the next subsection.

The characteristics of the PM_1P reflection observed under the western Iberian Massif suggest the existence of an increase in P-wave velocity with depth produced by a band of heterogeneities at approximately 55-85 km, depending on the tectonic zone. Several long-range controlled source experiments imaged a positive impedance contrast boundary at 60-90 km depth [*Green and Hales*, 1968; *Hales*, 1969, 1972; *Hales et al.*, 1980] that were interpreted as the Hales discontinuity and attributed to the spinel-to-garnet phase transition. In the next subsection, we discuss whether the modelled PM_1P reflection could correspond to this feature.

7.1.1. An Image of the Hales Discontinuity in SW Iberia?

The characteristics of the PM_1P reflection observed under the western Iberian Massif suggest the existence of an increase in P-wave velocity with depth produced by a band of heterogeneities at approximately 55-85 km, depending on the tectonic zone. Several long-range controlled source experiments imaged a positive impedance contrast boundary at 60-90 km depth [*Green and Hales*, 1968; *Hales*, 1969, 1972; *Hales et al.*, 1980] that were interpreted as the Hales discontinuity and attributed to the spinel-to-garnet phase transition. In this section, we discuss whether the modelled PM_1P reflection could correspond to this feature.

The continental upper mantle is a complex ensemble of ultramafic and mafic rocks. Peridotites are ultramafic igneous rocks typically made of olivine (>40%), clinopyroxene, orthopyroxene and an aluminous phase (plagioclase, spinel or garnet, depending on P-T conditions [*Kushiro and Yoder*, 1966; *Green and Hibberson*, 1970; *O'Neill*, 1981]. Mafic rocks (<40% olivine) are present, though less abundant, in the upper mantle (*e.g.* eclogites and pyroxenites) and reflect the imprint of tectonic and magmatic processes [*Irving*, 1980; *Rudnick et al.*, 2000; *Carlson et al.*, 2005]. Among peridotites, lherzolites are very common, and represent a fertile mantle able to produce basaltic magmas [*McDonough and Rudnick*, 1998].

The spinel-garnet transition is a critical reaction in the mantle. However, experimental investigations in natural compositional space are limited and incomplete [*e.g. Green and Ringwood*, 1967b; *Fumagalli and Klemme*, 2015, and references therein]. Experimental research around simple compositional systems like CMAS (CaO-MgO-Al_2O_3-SiO_2) and thermodynamic modeling have provided some constraints [*O'Neill*, 1981; *Perkins and Newton*, 1981; *Klemme and O'Neill*, 2000; *Klemme*, 2004; *Ziberna et al.*, 2013]. Apart from pressure and temperature, garnet stability is sensitive to mantle composition. That is, for fertile peridotites, like lherzolites, the spinel-garnet transition may occur at ~45 km depth (~1.5 GPa) whereas in refractory peridotites (*e.g.* dunites) the transition does not occur at depths shallower than ~90 km (~3.0 GPa) [*O'Neill*, 1981]. The addition of elements like Cr and Fe has a relevant effect on the system, elevating and reducing the garnet stability pressure, respectively [*O'Neill*, 1981; *Girnis and Brey*, 1999].

Volcanic mantle xenoliths provide direct petrological and chemical information about the mantle [*Pearson et al.*, 2014]. As an independent approach (yet, complementary to the seismic data), we utilized the chemical information of the closest mantle xenoliths from the Late Miocene-Quaternary Calatrava Volcanic Field (CVF, Fig. 1; [*Bianchini et al.*, 2010]) to

constrain the nearby upper mantle characteristics. Lherzolites with olivine, two pyroxenes, and spinel are common in the CVF xenoliths, whereas garnet is absent in all xenoliths. We explored the peridotitic parental magma pressure (P) and temperature (T) by applying thermodynamical modeling (MELTS, *Ghiorso and Sack* [1995]), as well as the classical geothermobarometric equations of *Putirka* [2008] and *Albarede* [1992] by utilizing the bulk compositions of peridotite xenoliths from *Villaseca et al.* [2010] (samples 58498 and 72672 of Cerro Pelado), and *Bianchini et al.* [2010] (sample CLV8). Results at 1000-1300°C indicate P in the range of 22-27 kbar (i.e. c. 65-80 km depth) and no garnet formation in the paragenesis, in line with the rocks information and previous estimations of the depth of xenolith extraction and LAB's depth (ca. 70-80 km; *Villaseca et al.* [2010]; *Villaseca et al.* [2019]). In this regard, in a simple compositional space (CMAS+Cr; *O'Neill* [1981]) the stability of spinel expands over higher pressures as a function of Cr (Cr#=[Cr/(Cr/Al)]. Spinels in lherzolites of the CVF depict a Cr# range = 0.09 – 0.21, with a mean value *ca*. Cr# = 0.14 [*Bianchini et al.*, 2010; *Villaseca et al.*, 2010]. For those values, the spinel-garnet transition could be expected between 21 and 24.5 kbar [*O'Neill*, 1981]. On the other hand, phase transition may occur in the reflectors range - between 50-85km (*ca.* 15-22 kbar) - only if spinel Cr# < 0.05 [*O'Neill*, 1981]. Upper mantle composition is heterogeneous where a small chemical element variation can modify the phase transition boundary [*Fumagalli and Klemme*, 2015]. Besides, geochemistry of the mantle below CVF presents a complex metasomatic imprint, tentatively related to long-term recycling of mafic rocks through an ancient subduction system (400-500 Ma; *Wilson and Downes* 1991; *Bianchini et al.*, 2010). This and the fact that the CVF lies out of our study area, may explain the wide range of P values in both results, ours and in literature.

The example provided above exhibits how lateral compositional changes in the upper-mantle, like elemental variation and/or fertility degree [*Barbero and Villaseca*, 2000; *Zeck et al.*, 2007; *Villaseca et al.*, 2012, 2015] could be invoked to explain different conditions (and depth) for the spinel-garnet transition. On the other side, taking into consideration the uncertainties on mantle thermobarometry [*Fumagalli and Klemme*, 2015; *MacGregor*, 2015], xenoliths from the CVF could be close to the spinel-garnet transformation. Also, they might be recording an old subduction environment, supporting the likely existence of eclogites in the upper mantle below the OMZ-CIZ transect. These findings would correlate with the presence of eclogite relicts exhumed in the Spanish Central System from ca. 50-60 km depth (15-19 kbar; [*Barbero and Villaseca*, 2000; *Gómez-Pugnaire et al.*, 2003; *Sánchez-Vizcaíno et al.*, 2003; *Pereira et al.*, 2010; *Villaseca et al.*, 2015]), thus indicating the heterogeneous mantle behavior.

Some authors relate the Hales discontinuity to anisotropy [*Fuchs*, 1983; *Zhang and Lay*, 1993; *Bostock*, 1997, 1998; *Levin and Park*, 2000; *Saul et al.*, 2000; *Musacchio et al.*, 2004]. In fact, *Díaz et al.* [1993] reported azimuthal anisotropy for the lithospheric mantle beneath the OMZ. Hence, anisotropy could play a role in the interpretation of the observed subcrustal reflectivity. Velocity anisotropy in the mantle is usually related to the preferred orientation of olivine [e.g. *Nicolas and Christensen*, 1987; *Ismaïl and Mainprice*, 1998]. However, the link between the Hales discontinuity and anisotropy is unknown, and different explanations have been proposed according to the tectonics of the area. *Bostock* [1997] proposed that, in the Canadian Slave Craton, this reflector could respond, among other things, to localized strain-induced anisotropy due to weakening by the phase change. On the other side, *Díaz et al.* [1993] relate the lithospheric anisotropy beneath the OMZ to shear zones that accommodate

the strain due to the decoupling between crust and mantle. Fast polarization direction on the active areas marks the direction of the present-day strain, whereas in zones with no tectonic activity the lattice preferred orientation develops as a result of the strain from the latest dynamic process affecting the region. Western Iberia has been basically stable since the late Paleozoic, hence mantle lithospheric anisotropy must be related to past events. SKS studies indicate a fast polarization in the ENE-WSW direction beneath the Iberian Peninsula [*Díaz and Gallart*, 2014] in agreement with the direction of the structures in the OMZ and CIZ. Anisotropy obtained by the ILIHA-DSS profiles indicates a N-S fast direction for the mantle lithosphere [*Díaz et al.*, 1996] although sampling is limited to the direction of the profiles. Accordingly, constraints provided by anisotropic studies in the area are not conclusive, regarding direction and depth where it occurs. Moreover, the observed anisotropy would have an effect on velocity and travel times and probably not so much in reflectivity.

In order to explain the observed reflections, our model defines a stochastic distribution of elliptical/elongated bodies. As discussed before, this model represents a heterogeneous gradient zone where the spinel-garnet phase transition (or, maybe, eclogite relics) occurs gradually and is the source of a lithological heterogeneity. Each inhomogeneity acts as a secondary source of reflectivity when excited by the primary wave radiating energy in all possible directions, generating constructive interference and enhancing the seismic signal. As a result, the seismic wavefield is strongly affected and ends up being a source of high random reflectivity. Therefore, we propose a model for the SW-Iberia with heterogeneities between 150 and 200 m thick within a 30 km thick gradient zone that ranges from 55-85 km depth. The heterogeneity bands create constructive interferences when thicknesses < 150 m and these build up the observed amplitudes and coda.

Although the phase change from spinel-peridotite to garnet-peridotite might have a too low reflection coefficient to explain the observed reflections [*Warner and McGeary*, 1987], layering or lenses with considerable spinel and garnet ratio variations could account for the observed reflectivity. A similar effect appears when the peridotite - eclogite pair is explored [*Chian et al.*, 1998; *Hansen and Balling*, 2004; *Wang et al.*, 2009; *Clowes et al.*, 2010; *Worthington et al.*, 2013]. Vp ranges for both (peridotite and eclogite) overlap for a wide range of contexts, which could lead to relatively low-velocity contrasts ($\Delta Vp < 1\%$) [*Kern et al.*, 1999; *Mauler et al.*, 2000; *Brown et al.*, 2009; *Wang et al.*, 2009; *Worthington et al.*, 2013]. However, even with such low-velocity contrast, a lamellar structure with alternation of eclogites and peridotites could account for the observed reflectivity. At this point, the proposed model features a lamellar nature of the upper mantle between 55-85 km, seismically compatible with the Hales discontinuity. Whether these heterogeneities are the result of either erratic spinel-garnet transformation, a long-run mixture of eclogites and peridotites or both, must be settled with further investigations (e.g. Vp/Vs; *Worthington et al.*, 2013; *Farla et al.*, 2017). However, the size and position of the reflector favor an origin linked to a phase transition.

7.2. SW Iberia Lithosphere-Asthenosphere Boundary (LAB): The PM_2P Phase

A reflector deeper than that imaged by PM_1P is observed in the ALCUDIA-WA and ILIHA-DSS surveys, and also in the later inspections of the IBERSEIS-WA dataset. This reflector (linked to PM_2P) features a decrease in Vp with depth from 8.3 to 8.0 km/s, and its location and geometry are also variable across the different tectonic zones (Figure 8). Beneath the OMZ it is located at

90 km depth (ILIHA line DA and CF, Figure 7a and c), deepening to the south down to 100 km depth (ILIHA line BX, Figure 7b). On the other side, this interface presents a variable topography beneath the CIZ. The ALCUDIA-WA survey images this interface at 105-110 km depth (Figure 6) beneath its southeastern part, meanwhile further to the northwest it shallows up to 80 km depth (ILIHA line BE, Figure 7).

We postulate that this PM_2P reflector corresponds to the base of the lithosphere, the so-called LAB. Recent active source seismic studies have imaged the base of the tectonic (lithospheric) plate [*Stern et al.*, 2014] as a negative reflection coefficient interface in accordance with our dataset where the observed PM_2P phase features negative polarity. This study also concludes that the velocity change occurs over a thickness of less than 1 km. The nature of the here presented PM_2P reflection (dominant frequency of 8 Hz) and the modeled upper mantle velocity of 8.3 km/s indicates that the decrease in velocity takes place in a zone thinner than 1 km as well. The resulting synthetic seismograms (Figure 9) reproduce its travel time, offset, and amplitude as coming from a decrease in velocity at the proposed depths, reinforcing this interpretation. Our results indicate that the transition from the lithosphere to the asthenosphere beneath the Iberian Massif is produced by a rapid vertical P-wave velocity decrease. Such velocity change defines a LAB characterized by a change in the elastic properties of the rocks produced over a small depth interval. Such thin gradient zone can be explained not only for the rise of temperature and change in composition with depth but by the presence of partial melt at the base of the lithosphere [*Fischer*, 2015 and references therein].

Geophysical studies on surface wave tomography place the LAB at ~90 km depth beneath the OMZ, at 80-90 on the southwest CIZ, and at ~70 km on the northeast CIZ [*Palomeras et al.*, 2017]. Differences between this study and our results are on average around 5 km although locally, to the southwest CIZ they increase up to 15 km. Discrepancies on the LAB depth obtained by different geophysical techniques have been reported [*Eaton et al.*, 2009]. Surface wave tomography provides depth-velocity models that are relatively insensitive to the sharpness of the LAB, being unable to distinguish a velocity change that occurs instantaneously in depth and one occurring over tens of kilometers [*Eaton et al.*, 2009]. This conditions the definition of the LAB, which *Palomeras et al.* [2017] took as the maximum negative velocity gradient below a fast lid, which might not be necessarily the point with the maximum impedance contrast and where reflections originate. Considering the LAB as the depth to a certain absolute velocity or a velocity anomaly contour, or the depth where lateral velocity variations cease, would lead to different LAB depths for the Iberian Peninsula. This could explain the discrepancies of 5 km (locally up to ~15 km) obtained by surface-wave tomography analysis and the ALCUDIA and ILIHA models presented in this study.

Other geophysical studies using elevation, geoid, and gravity data [*Palomeras et al.*, 2011], and topography and geoid data [*Torne et al.*, 2015], report similar LAB depths for the CIZ (90 km) as the ones interpreted in the wide-angle seismic profiles presented here. These studies also increase the LAB depth beneath the southwest CIZ up to 110 km depth, in agreement with the results obtained in this study. The main differences arise beneath the northeast CIZ, where *Torne et al.* [2015] report a LAB depth of 110 km whereas our model places it at 80 km depth. However, this lithospheric thinning is in agreement with that observed in the surface wave tomography results [*Palomeras et al.*, 2017]. In summary, the topography of the LAB presented in this work is in general in agreement with that obtained by other geophysical data.

9 Conclusions

Modeling of different refraction/wide-angle seismic datasets identifies a heterogeneous upper mantle beneath the Spanish Iberian Massif, with at least two sub-Moho reflectors. The studied profiles image an upper mantle reflection, PM_1P, produced by an increase in P-wave velocity at ~55-85 km depth beneath the OMZ that shallows up to 50-60 km beneath the CIZ (Figure 8). The characteristics of this phase (coda and amplitude) indicate that it corresponds to a band of heterogeneities randomly distributed with $\Delta Vp=\pm 0.1$ km/s. Due to its depth and geological constraints, we postulate that this interface could correspond to the transition zone from spinel to garnet lherzolite, although the existence of a heterogeneous distribution of mafic bodies (e.g. eclogites, garnetites, pyroxenites) cannot be ruled out. The randomly distributed heterogeneities would correspond to either mechanical or chemical mixing, which led to variations on the spinel and garnet ratio. The geometry of this interface could be due to mantle elemental changes, fertility degree, and tectonothermal evolution. The interlayer spacing of this gradient zone determines its image in different datasets. The fact that the reflector is not sampled continuously in every dataset implies that it has lateral variations that modify its reflectivity depending on the characteristics of the sampling wavelet.

A second, deeper reflection has been observed in the shot gathers. Its reversed polarity and modeling indicate that it corresponds to a sharp decrease in velocity with depth. Our modeling study places this discontinuity around 90 km depth beneath the OMZ. A lateral change is observed beneath the CIZ, where it is imaged at 103-110 km depth on the southeast shallowing up to 80 km depth on the northeast. Furthermore, the imaged depth of this discontinuity agrees with the LAB depth obtained for the area by other geophysical observations. This indicates that it likely corresponds to the base of the lithosphere. The characteristics of this arrival depict a rapid change with depth of the rock properties at this boundary and/or the presence of partial melt at the base of the lithosphere.

Acknowledgments

The authors thank the Associated Editor and two anonymous reviewers for their thoroughly valuable suggestions and comments that improved the manuscript. This research was funded by the Spanish Ministry of Economy and Competitivity CGL2016-78560-P, the Junta de Castilla y León SA065P17, IP is funded by MCIU and USal (BEAGAL18/00090). JGB appreciates financial support from ILL (1-02-232 & 1-02-163) and superb technical assistance from T. Hansen and B. Ouladiaf. JA is funded by MICINN (Juan de la Cierva fellowship - IJC2018-036074-I). The figures in this paper were generated using the public domain Generic Mapping Tools (GMT) software [*Wessel and Smith, 1995*].

The data used in this work is accessible at the DIGITAL.CSIC repository [*DeFelipe et al.*, 2020]. ILIHA-DSS data is available at http://dx.doi.org/10.20350/digitalCSIC/12623, IBERSEIS-WA data is available at http://dx.doi.org/10.20350/digitalCSIC/9018; and ALCUDIA-WA data is available at http://dx.doi.org/10.20350/digitalCSIC/9061.

References

Abramovitz, T., H. Thybo, and M. L. W. Group (1998), Seismic structure across the Caledonian Deformation Front along MONA LISA profile 1 in the southeastern North Sea,

Tectonophysics, *288*(1–4), 153–176, doi:10.1016/S0040-1951(97)00290-4.

Aki, K., and P. G. Richards (2002), *Quantitative Seismology*, 2nd ed.

Albarede, F. (1992), How deep do common basaltic magmas form and differentiate?, *J. Geophys. Res.*, *97*(B7), 10997, doi:10.1029/91JB02927.

Alsdorf, D., L. Brown, and D. Nelson (1996), Possible upper mantle reflection fabric on seismic profiles from the Tethyan Himalaya: Identification and tectonic interpretation, *J. Geophys. Res.*, *101*(B11), 25305–25320.

Anand, A., D. K. Bora, K. Borah, and J. Madhab Borgohain (2017), Seismological evidence of the Hales discontinuity in northeast India, *J. Asian Earth Sci.*, doi:10.1016/j.jseaes.2017.12.015.

Andrés, J., D. Draganov, M. Schimmel, P. Ayarza, I. Palomeras, M. Ruiz, and R. Carbonell (2019), Lithospheric image of the Central Iberian Zone (Iberian Massif) using global-phase seismic interferometry, *Solid Earth*, *10*(6), 1937–1950, doi:10.5194/se-10-1937-2019.

Andrés, J., P. Ayarza, M. Schimmel, I. Palomeras, M. Ruiz, and R. Carbonell (2020), What can seismic noise tell us about the Alpine reactivation of the Iberian Massif? An example in the Iberian Central System, *Solid Earth*, doi:10.5194/se-2020-94.

Austrheim, H., M. Erambert, and A. K. Engvik (1997), Processing of crust in the root of the Caledonian continental collision zone: the role of eclogitization, *Tectonophysics*, *273*(1–2), 129–153, doi:10.1016/S0040-1951(96)00291-0.

Van Avendonk, H. J. A., W. S. Holbrook, D. Lizarralde, and P. Denyer (2011), Structure and serpentinization of the subducting Cocos plate offshore Nicaragua and Costa Rica, *Geochemistry, Geophys. Geosystems*, *12*(6), n/a-n/a, doi:10.1029/2011GC003592.

Ayarza, P., I. Palomeras, R. Carbonell, J. C. Afonso, and F. Simancas (2010), A wide-angle upper mantle reflector in SW Iberia: Some constraints on its nature, *Phys. Earth Planet. Inter.*, *181*(3–4), 88–102, doi:10.1016/j.pepi.2010.05.004.

Azor, A., D. Rubatto, J. F. Simancas, F. González Lodeiro, D. Martínez Poyatos, L. M. Martín Parra, and J. Matas (2008), Rheic Ocean ophiolitic remnants in southern Iberia questioned by SHRIMP U-Pb zircon ages on the Beja-Acebuches amphibolites, *Tectonics*, *27*(5), TC5006, doi:10.1029/2008TC002306.

Azor, A. et al. (2019), Deformation and Structure, in *The Geology of Iberia: A Geodynamic Approach*, edited by C. Quesada and J. T. Oliveira, pp. 307–348, Springer International Publishing.

BABEL Working Group (1990), Evidence for early proterozoic plate tectonics from seismic reflection profiles in the Baltic Shield, *Nature*, *348*(6296), 34–38, doi:10.1038/348034a0.

Ballèvre, M. et al. (2014), Correlation of the nappe stack in the Ibero-Armorican arc across the Bay of Biscay: a joint French–Spanish project, *Geol. Soc. London, Spec. Publ.*, *405*(1), 77–113, doi:10.1144/SP405.13.

Balling, N. (2000), Deep seismic reflection evidence for ancient subduction and collision zones within the continental lithosphere of Northwestern Europe, *Tectonophysics*, *329*(1–4), 269–

300, doi:10.1016/S0040-1951(00)00199-2.

Barbero, L., and C. Villaseca (2000), Eclogite facies relics in metabasites from the Sierra de Guadarrama (Spanish Central System): P-T estimations and implications for the Hercynian evolution, *Mineral. Mag.*, *64*(05), 815–836, doi:10.1180/002646100549814.

Bianchini, G., L. Beccaluva, C. Bonadiman, G. M. Nowell, D. G. Pearson, F. Siena, and M. Wilson (2010), Mantle metasomatism by melts of HIMU piclogite components: new insights from Fe-lherzolite xenoliths (Calatrava Volcanic District, central Spain), *Geol. Soc. London, Spec. Publ.*, *337*(1), 107–124, doi:10.1144/SP337.6.

Bostock, M. G. (1997), Anisotropic upper-mantle stratigraphy and architecture of the Slave craton, *Nature*, *390*(27 NOVEMBER), 392–395, doi:10.1038/37102.

Bostock, M. G. (1998), Mantle stratigraphy and evolution of the Slave province, *J. Geophys. Res. Solid Earth*, *103*(B9), 21183–21200, doi:10.1029/98JB01069.

Brown, D., S. Llana-Funez, R. Carbonell, J. Alvarez-Marron, D. Marti, and M. Salisbury (2009), Laboratory measurements of P-wave and S-wave velocities across a surface analog of the continental crust–mantle boundary: Cabo Ortegal, Spain, *Earth Planet. Sci. Lett.*, *285*(1–2), 27–38, doi:10.1016/j.epsl.2009.05.032.

Calvert, A. J. (2004), Seismic reflection imaging of two megathrust shear zones in the northern Cascadia subduction zone, *Nature*, *428*(6979), 163–167, doi:10.1038/nature02372.

Carbonell, R. (2004), On the nature of mantle heterogeneities and discontinuities: Evidence from a very dense wide-angle shot record, *Tectonophysics*, *388*(1-4 SPEC. ISS.), 103–117, doi:10.1016/j.tecto.2004.07.025.

Carlson, R. W., D. G. Pearson, and D. E. James (2005), Physical, chemical, and chronological characteristics of continental mantle, *Rev. Geophys.*, *43*(1), 1–24, doi:10.1029/2004RG000156.

Chapman, C. (2004), *Fundamentals of Seismic Wave Propagation*, Cambridge University Press.

Chian, D., F. Marillier, J. Hall, and G. Quinlan (1998), An improved velocity model for the crust and upper mantle along the central mobile belt of the Newfoundland Appalachian orogen and its offshore extension, *Can. J. Earth Sci.*, *35*(11), 1238–1251, doi:10.1139/e98-042.

Clowes, R. M., D. J. White, and Z. Hajnal (2010), Mantle heterogeneities and their significance: results from Lithoprobe seismic reflection and refraction - wide-angle reflection studies, *Can. J. Earth Sci.*, *47*(5), 409–443, doi:10.1139/E10-003.

Cook, F. A., A. J. Van Der Velden, K. W. Hall, and B. J. Roberts (1999), Frozen subduction in Canada's Northwest Territories: Lithoprobe deep lithospheric reflection profiling of the western Canadian Shield, *Tectonics*, *18*(1), 1–24, doi:10.1029/1998TC900016.

Cook, F. A., R. M. Clowes, D. B. Snyder, A. J. van der Velden, K. W. Hall, P. Erdmer, and C. A. Evenchick (2004), Precambrian crust beneath the Mesozoic northern Canadian Cordillera discovered by Lithoprobe seismic reflection profiling, *Tectonics*, *23*(2), 1–28, doi:10.1029/2002TC001412.

DeFelipe, I. et al. (2020), Reassessing the lithosphere: SeisDARE, an open access seismic data

repository, *Earth Syst. Sci. Data Discuss.*, *2020*, 1–32, doi:https://doi.org/10.5194/essd-2020-208.

Dias da Silva, Í., M. F. Pereira, J. B. Silva, and C. Gama (2018), Time-space distribution of silicic plutonism in a gneiss dome of the Iberian Variscan Belt: The Évora Massif (Ossa-Morena Zone, Portugal), *Tectonophysics*, *747–748*, 298–317, doi:10.1016/j.tecto.2018.10.015.

Diaz, J., J. Gallart, and R. Carbonell (2016), Moho topography beneath the Iberian-Western Mediterranean region mapped from controlled-source and natural seismicity surveys, *Tectonophysics*, *692*, 74–85, doi:10.1016/j.tecto.2016.08.023.

Díaz, J., and J. Gallart (2014), Seismic anisotropy from the Variscan core of Iberia to the Western African Craton: New constrains on upper mantle flow at regional scales, *Earth Planet. Sci. Lett.*, *394*, 48–57, doi:10.1016/j.epsl.2014.03.005.

Díaz, J., A. Hirn, J. Gallart, and L. Senos (1993), Evidence for azimuthal anisotropy in southwest Iberia from deep seismic sounding data, *Phys. Earth Planet. Inter.*, *78*, 193–206.

Díaz, J., A. Hirn, J. Gallart, and B. Abalos (1996), Upper-mantle anisotropy in SW Iberia from long-range seismic profiles and teleseismic shear-wave data, *Phys. Earth Planet. Inter.*, *9201*(95).

Eaton, D. W., F. Darbyshire, R. L. Evans, H. Grütter, A. G. Jones, and X. Yuan (2009), The elusive lithosphere–asthenosphere boundary (LAB) beneath cratons, *Lithos*, *109*(1–2), 1–22, doi:10.1016/j.lithos.2008.05.009.

Ehsan, S. A., R. Carbonell, P. Ayarza, D. Martí, A. Pérez-Estaún, D. J. Martínez-Poyatos, J. F. Simancas, A. Azor, and L. Mansilla (2014), Crustal deformation styles along the reprocessed deep seismic reflection transect of the Central Iberian Zone (Iberian Peninsula), *Tectonophysics*, *621*, 159–174, doi:10.1016/j.tecto.2014.02.014.

Ehsan, S. A., R. Carbonell, P. Ayarza, D. Martí, D. Martínez Poyatos, J. F. Simancas, A. Azor, C. Ayala, M. Torné, and A. Pérez-Estaún (2015), Lithospheric velocity model across the Southern Central Iberian Zone (Variscan Iberian Massif): The ALCUDIA wide-angle seismic reflection transect, *Tectonics*, *34*(3), 535–554, doi:10.1002/2014TC003661.

Farla, R., A. Rosenthal, C. Bollinger, S. Petitgirard, J. Guignard, N. Miyajima, T. Kawazoe, W. A. Crichton, and D. J. Frost (2017), High-pressure, high-temperature deformation of dunite, eclogite, clinopyroxenite and garnetite using in situ X-ray diffraction, *Earth Planet. Sci. Lett.*, *473*, 291–302, doi:10.1016/j.epsl.2017.06.019.

Fernández Viejo, G., and R. M. Clowes (2003), Lithospheric structure beneath the Archaean Slave Province and Proterozoic Wopmay orogen, northwestern Canada, from a LITHOPROBE refraction/wide-angle reflection survey, *Geophys. J. Int.*, *153*(1), 1–19, doi:10.1046/j.1365-246X.2003.01807.x.

Fischer, K. M. (2015), Crust and Lithospheric Structure - Seismological Constraints on the Lithosphere-Asthenosphere Boundary, in *Treatise on Geophysics*, edited by B. A. Romanowicz and A. M. Dziewonski, pp. 587–612, Elsevier B.V., Amsterdam, The Netherlands.

Fonseca, P., and A. Ribeiro (1993), Tectonics of the Beja-Acebuches Ophiolite: a major suture in the Iberian Variscan Foldbelt, *Geol. Rundschau*, *82*(3), 440–447, doi:10.1007/BF00212408.

Fountain, D. M., C. A. Hurich, and S. B. Smithson (1984), Seismic reflectivity of mylonite zones in the crust, *Geology*, *12*(4), 195, doi:10.1130/0091-7613(1984)12<195:SROMZI>2.0.CO;2.

Frederiksen, S., and J. Braun (2001), Numerical modelling of strain localisation during extension of the continental lithosphere, *Earth Planet. Sci. Lett.*, *188*(1–2), 241–251, doi:10.1016/S0012-821X(01)00323-5.

Fuchs, K. (1983), Recently formed elastic anisotropy and petrological models for the continental subcrustal lithosphere in southern Germany, *Phys. Earth Planet. Inter.*, *31*(2), 93–118, doi:10.1016/0031-9201(83)90103-6.

Fuchs, K., M. Tittgemeyer, T. Ryberg, F. Wenzel, and W. D. Mooney (2002), Global significance of a sub-Moho boundary layer (SMBL) deduced from high-resolution seismic observations, *Int. Geol. Rev.*, *44*(8), 671–685, doi:10.2747/0020-6814.44.8.671.

Fumagalli, P., and S. Klemme (2015), Mineralogy of the Earth: Phase Transitions and Mineralogy of the Upper Mantle, in *Treatise on Geophysics*, vol. 2, edited by G. Schubert, pp. 7–31, Elsevier, Oxford, Oxford.

Ghiorso, M. S., and R. O. Sack (1995), Chemical mass transfer in magmatic processes IV. A revised and internally consistent thermodynamic model for the interpolation and extrapolation of liquid-solid equilibria in magmatic systems at elevated temperatures and pressures, *Contrib. to Mineral. Petrol.*, *119*(2–3), 197–212, doi:10.1007/BF00307281.

Girardeau, J., J. I. G. Ibarguchi, and N. Ben Jamaa (1989), Evidence for a heterogeneous upper mantle in the Cabo Ortegal Complex, Spain, *Science (80-.).*, *245*(4923), 1231–1233, doi:10.1126/science.245.4923.1231.

Girnis, A. V., and G. P. Brey (1999), Garnet-spinel-olivine-orthopyroxene equilibria in the FeO-MgO-Al2O3-SiO2-Cr2O3 system: II. Thermodynamic analysis, *Eur. J. Mineral.*, *11*(4), 619–636, doi:10.1127/ejm/11/4/0619.

Gómez-Pugnaire, M. T., A. Azor, J. M. Fernández-Soler, and V. López Sánchez-Vizcaíno (2003), The amphibolites from the Ossa-Morena/Central Iberian Variscan suture (Southwestern Iberian Massif): Geochemistry and tectonic interpretation, *Lithos*, *68*(1–2), 23–42, doi:10.1016/S0024-4937(03)00018-5.

Gomez Barreiro, J., S. Barrios Sanchez, J. M. Benitez Perez, Y. El Mendily, L. Lutterotti, J. Morales, B. Ouladdiaf, M. Tettamanti, and M. Zucali (2018), Texture-induced anisotropy as a seismic tectonic flow fingerprint, , doi:10.5291/ILL-DATA.1-02-232.

Gómez Barreiro, J., J. R. Martínez Catalán, D. Prior, H. -R. Wenk, S. Vogel, F. Díaz García, R. Arenas, S. Sánchez Martínez, and I. Lonardelli (2010), Fabric Development in a Middle Devonian Intraoceanic Subduction Regime: The Careón Ophiolite (Northwest Spain), *J. Geol.*, *118*(2), 163–186, doi:10.1086/649816.

Gómez Barreiro, J., H.-R. Wenk, and S. Vogel (2015), Texture and elastic anisotropy of a mylonitic anorthosite from the Morin Shear Zone (Quebec, Canada), *J. Struct. Geol.*, *71*,

100–111, doi:10.1016/j.jsg.2014.07.021.

Gorman, A. R. et al. (2002), Deep Probe: imaging the roots of western North America, *Can. J. Earth Sci.*, *39*(3), 375–398, doi:10.1139/e01-064.

Green, D. H., and W. Hibberson (1970), The instability of plagioclase in peridotite at high pressure, *Lithos*, *3*(3), 209–221, doi:10.1016/0024-4937(70)90074-5.

Green, D. H., and A. E. Ringwood (1967a), An experimental investigation of the gabbro to eclogite transformation and its petrological applications, *Geochim. Cosmochim. Acta*, *31*(5), 767–833, doi:10.1016/S0016-7037(67)80031-0.

Green, D. H., and A. E. Ringwood (1967b), The stability fields of aluminous pyroxene peridotite and garnet peridotite and their relevance in upper mantle structure, *Earth Planet. Sci. Lett.*, *3*(C), 151–160, doi:10.1016/0012-821X(67)90027-1.

Green, R. W. E., and A. L. Hales (1968), The travel times of P waves to 30° in the central United States and upper mantle structure, *Bull. Seismol. Soc. Am.*, *58*(1), 267–289.

Griffin, W. L., S. Y. O'Reilly, J. C. Afonso, and G. C. Begg (2009), The Composition and Evolution of Lithospheric Mantle: a Re-evaluation and its Tectonic Implications, *J. Petrol.*, *50*(7), 1185–1204, doi:10.1093/petrology/egn033.

Hacker, B. R. (1996), Eclogite formation and the rheology, buoyancy, seismicity, and H2O content of oceanic crust, in *Geophysical Monograph Series*, vol. 96, pp. 337–346.

Hajnal, Z., B. Nemeth, R. M. Clowes, R. M. Ellis, G. D. Spence, M. J. a. Burianyk, I. Asudeh, D. J. White, and D. a. Forsyth (1997), Mantle involvement in lithospheric collision: Seismic evidence from the Trans-Hudson Orogen, western Canada, *Geophys. Res. Lett.*, *24*(16), 2079, doi:10.1029/97GL01958.

Hales, A. L. (1969), A seismic discontinuity in the lithosphere, *Earth Planet. Sci. Lett.*, *7*(July), 44–46.

Hales, A. L. (1972), The travel times of P seismic waves and their relevance to the upper mantle velocity distribution, *Tectonophysics*, *13*(1–4), 447–482.

Hales, A. L., K. J. Muirhead, and J. R. Rynn (1980), A compressional velocity distribution for the upper mantle, *Tectonophysics*, *63*, 309–348.

Hammer, P. T. C., and R. M. Clowes (2004), Accreted terranes of northwestern British Columbia, Canada: Lithospheric velocity structure and tectonics, *J. Geophys. Res. Solid Earth*, *109*(6), 1–19, doi:10.1029/2003JB002749.

Hansen, T. M., and N. Balling (2004), Upper-mantle reflectors: Modelling of seismic wavefield characteristics and tectonic implications, *Geophys. J. Int.*, *157*(2), 664–682, doi:10.1111/j.1365-246X.2004.02217.x.

Holliger, K., and A. R. Levander (1992), A stochastic view of lower crustal fabric based on evidence from the Ivrea Zone, *Geophys. Res. Lett.*, *19*(11), 1153–1156, doi:10.1029/92GL00919.

Iliha DSS Group (1993), A deep seismic sounding investigation of lithospheric heterogeneity and anisotropy beneath the Iberian Peninsula, *Tectonophysics*, *221*, 35–51.

Irving, A. (1980), Petrology and geochemistry of composite ultramafic xenoliths in alkalic basalts and implications for magmatic processes within the mantle, *Am. J. Sci.*, *280*(2), 389–426.

Ismaïl, W. Ben, and D. Mainprice (1998), An olivine fabric database: an overview of upper mantle fabrics and seismic anisotropy, *Tectonophysics*, *296*(1–2), 145–157, doi:10.1016/S0040-1951(98)00141-3.

Ito, K., and G. C. Kennedy (1971), An Experimental Study of the Basalt-Garnet Granulite-Eclogite Transition, in *The Structure and Physical Properties of the Earth's Crust*, edited by John G. Heacock, pp. 303–314.

Kennett, B. L. N., and E. R. Engdahl (1991), Traveltimes for global earthquake location and phase identification, *Geophys. J. Int.*, *105*(2), 429–465, doi:10.1111/j.1365-246X.1991.tb06724.x.

Kennett, B. L. N., E. R. Engdah, and R. Buland (1995), Constraints on seismic velocities in the Earth from traveltimes, *Geophys. J. Int.*, *122*, 108–124.

Kern, H., S. Gao, Z. Jin, T. Popp, and S. Jin (1999), Petrophysical studies on rocks from the Dabie ultrahigh-pressure (UHP) metamorphic belt, Central China: Implications for the composition and delamination of the lower crust, *Tectonophysics*, *301*(3–4), 191–215, doi:10.1016/S0040-1951(98)00268-6.

Klemme, S. (2004), The influence of Cr on the garnet–spinel transition in the Earth's mantle: experiments in the system MgO–Cr2O3–SiO2 and thermodynamic modelling, *Lithos*, *77*(1–4), 639–646, doi:10.1016/j.lithos.2004.03.017.

Klemme, S., and H. S. C. O'Neill (2000), The near-solidus transition from garnet lherzolite to spinel lherzolite, *Contrib. to Mineral. Petrol.*, *138*(3), 237–248, doi:10.1007/s004100050560.

Kushiro, I., and H. S. Yoder (1966), Anorthite - forsterite and anorthite - enstatite reactions and their bearing on the basalt - eclogite transformation, *J. Petrol.*, *7*(3), 337–362, doi:10.1093/petrology/7.3.337.

Levin, V., and J. Park (2000), Shear zones in the Proterozoic lithosphere of the Arabian shield and the nature of the Hales discontinuity, *Tectonophysics*, *323*(3–4), 131–148, doi:10.1016/S0040-1951(00)00105-0.

MacGregor, I. D. (2015), Empirical geothermometers and geothermobarometers for spinel peridotite phase assemblages, *Int. Geol. Rev.*, *57*(15), 1940–1974, doi:10.1080/00206814.2015.1045307.

Martinez Catalan, J. R. (2011), Are the oroclines of the Variscan belt related to late Variscan strike-slip tectonics?, *Terra Nov.*, *23*(4), 241–247, doi:10.1111/j.1365-3121.2011.01005.x.

Martínez Catalán, J. R. (2012), The Central Iberian arc, an orocline centered in the Iberian Massif and some implications for the Variscan belt, *Int. J. Earth Sci.*, *101*(5), 1299–1314, doi:10.1007/s00531-011-0715-6.

Martínez Catalán, J. R. et al. (2007), Space and time in the tectonic evolution of the northwestern Iberian Massif: Implications for the Variscan belt, in *Memoir of the Geological Society of*

America, vol. 200, pp. 403–423, Geological Society of America.

Martínez Catalán, J. R. et al. (2019), Variscan Suture Zone and Suspect Terranes in the NW Iberian Massif: Allochthonous Complexes of the Galicia-Trás os Montes Zone (NW Iberia), in *The Geology of Iberia: A Geodynamic Approach*, edited by C. Quesada and J. T. Oliveira, pp. 99–130, Springer International Publishing.

Martínez Poyatos, D. et al. (2012), Imaging the crustal structure of the Central Iberian Zone (Variscan Belt): The ALCUDIA deep seismic reflection transect, *Tectonics*, *31*(3), TC3017, doi:10.1029/2011TC002995.

Massé, R. P. (1987), Crustal and upper mantle structure of stable continental regions in North America and northern Europe, *Pure Appl. Geophys. PAGEOPH*, *125*(2–3), 205–239, doi:10.1007/BF00874495.

Mauler, A., L. Burlini, K. Kunze, P. Philippot, and J. P. Burg (2000), P-wave anisotropy in eclogites and relationship to the omphacite crystallographic fabric, *Phys. Chem. Earth, Part A Solid Earth Geod.*, *25*(2), 119–126, doi:10.1016/S1464-1895(00)00020-X.

McDonough, W. F., and R. L. Rudnick (1998), Chapter 4. MINERALOGY AND COMPOSITION OF THE UPPER MANTLE, in *Ultrahigh Pressure Mineralogy: Physics and Chemistry of the Earth's Deep Interior*, edited by R. J. Hemley, pp. 139–164, De Gruyter, Berlin, Boston.

Medaris, L. G., H. K. Brueckner, Y. Cai, W. L. Griffin, and M. Janák (2018), Eclogites in peridotite massifs in the Western Gneiss Region, Scandinavian Caledonides: Petrogenesis and comparison with those in the Variscan Moldanubian Zone, *Lithos*, *322*, 325–346, doi:10.1016/j.lithos.2018.10.013.

Meissner, R. (1989), Rupture, creep, lamellae and crocodiles: happenings in the continental crust, *Terra Nov.*, *1*(1), 17–28, doi:10.1111/j.1365-3121.1989.tb00321.x.

MONA LISA Working Group (1997), MONA LISA - Deep seismic investigations of the lithosphere in the southeastern North Sea, *Tectonophysics*, *269*(1–2), 1–19, doi:10.1016/S0040-1951(96)00111-4.

Morozov, I. B., and S. B. Smithson (2000), Coda of long-range arrivals from nuclear explosions, *Bull. Seismol. Soc. Am.*, *90*(4), 929–939, doi:10.1785/0119990125.

Morozov, I. B., E. A. Morozova, S. B. Smithson, and L. N. Solodilov (1998), On the nature of the teleseismic Pn phase observed on the ultralong-range profile "Quartz," Russia, *Bull. Seismol. Soc. Am.*, *88*(1), 62–73.

Musacchio, G., D. J. White, I. Asudeh, and C. J. Thomson (2004), Lithospheric structure and composition of the Archean western Superior Province from seismic refraction/wide-angle reflection and gravity modeling, *J. Geophys. Res.*, *109*(B3), B03304, doi:10.1029/2003JB002427.

Nicolas, A., and N. I. Christensen (1987), Formation of Anisotropy in Upper Mantle Peridotites - A Review, in *Composition, Structure and Dynamics of the Lithosphere-Asthenosphere System*, edited by K. Fuchs and C. Froidevaux, pp. 111–123, American Geophysical Union.

Nielsen, L., H. Thybo, A. Levander, and L. N. Solodilov (2003), Origin of upper-mantle seismic

scattering - Evidence from Russian peaceful nuclear explosion data, *Geophys. J. Int.*, *154*(1), 196–204, doi:10.1046/j.1365-246X.2003.01955.x.

O'Neill, H. S. C. (1981), The transition between spinel lherzolite and garnet lherzolite, and its use as a Geobarometer, *Contrib. to Mineral. Petrol.*, *77*(2), 185–194, doi:10.1007/BF00636522.

Palomeras, I., R. Carbonell, I. Flecha, F. Simancas, P. Ayarza, J. Matas, D. Martínez Poyatos, A. Azor, F. González-Lodeiro, and A. Pérez-Estaún (2009), Nature of the lithosphere across the Variscan orogen of SW Iberia: Dense wide-angle seismic reflection data, *J. Geophys. Res.*, *114*(B2), 1–29, doi:10.1029/2007JB005050.

Palomeras, I., R. Carbonell, P. Ayarza, M. Fernàndez, J. F. Simancas, D. M. Poyatos, F. González Lodeiro, and A. Pérez-Estaún (2011), Geophysical model of the lithosphere across the Variscan Belt of SW-Iberia: Multidisciplinary assessment, *Tectonophysics*, *508*(1–4), 42–51, doi:10.1016/j.tecto.2010.07.010.

Palomeras, I., S. Thurner, A. Levander, K. Liu, A. Villasenor, R. Carbonell, and M. Harnafi (2014), Finite-frequency Rayleigh wave tomography of the western Mediterranean: Mapping its lithospheric structure, *Geochemistry, Geophys. Geosystems*, *15*(1), 140–160, doi:10.1002/2013GC004861.

Palomeras, I., A. Villaseñor, S. Thurner, A. Levander, J. Gallart, and M. Harnafi (2017), Lithospheric structure of Iberia and Morocco using finite-frequency Rayleigh wave tomography from earthquakes and seismic ambient noise, *Geochemistry, Geophys. Geosystems*, *18*(5), 1824–1840, doi:10.1002/2016GC006657.

Pavlenkova, N. I. (1996), General features of the uppermost mantle stratification from long-range seismic profiles, *Tectonophysics*, *264*(1–4), 261–278, doi:http://dx.doi.org/10.1016/S0040-1951(96)00131-X.

Pearson, D. G., D. Canil, and S. B. Shirey (2014), Mantle Samples Included in Volcanic Rocks, in *Treatise on Geochemistry*, vol. 3, pp. 169–253, Elsevier.

Pereira, M. F., A. Apraiz, M. Chichorro, J. B. Silva, and R. A. Armstrong (2010), Exhumation of high-pressure rocks in northern Gondwana during the Early Carboniferours (Coimbra-Cordoba shear zone, SW Iberian Massif): Tectonothermal analysis and U-Th-Pb SHRIMP in-situ zircon geochronology, *Gondwana Res.*, *17*(2–3), 440–460, doi:10.1016/j.gr.2009.10.001.

Perkins, D., and R. C. Newton (1981), The compositions of coexisting pyroxenes and garnet in the system CaO-MgO-Al2O3-SiO2 at 900º-1,100º C and high pressures, *Contrib. to Mineral. Petrol.*, *75*(3), 291–300, doi:10.1007/BF01166769.

Putirka, K. D. (2008), Thermometers and Barometers for Volcanic Systems, *Rev. Mineral. Geochemistry*, *69*(1), 61–120, doi:10.2138/rmg.2008.69.3.

Quesada, C., J. A. Braid, P. Fernandes, P. Ferreira, R. S. Jorge, J. X. Matos, J. B. Murphy, J. T. Oliveira, J. Pedro, and Z. Pereira (2019), SW Iberia Variscan Suture Zone: Oceanic Affinity Units, in *The Geology of Iberia: A Geodynamic Approach*, edited by C. Quesada and J. T. Oliveira, pp. 131–171, Springer.

Revenaugh, J., and T. H. Jordan (1991), Mantle layering from ScS reverberations: 3. The upper mantle, *J. Geophys. Res. Solid Earth*, *96*(B12), 19781–19810, doi:10.1029/91JB01487.

Rudnick, R. L., M. Barth, I. Horn, and W. F. McDonough (2000), Rutile-Bearing Refractory Eclogites: Missing Link Between Continents and Depleted Mantle, *Science (80-.).*, *287*(5451), 278–281, doi:10.1126/science.287.5451.278.

Sánchez-Vizcaíno, V. L., M. T. Gómez-Pugnaire, A. Azor, and J. M. Fernández-Soler (2003), Phase diagram sections applied to amphibolites: A case study from the Ossa-Morena/Central Iberian Variscan suture (Southwestern Iberian Massif), *Lithos*, *68*(1–2), 1–21, doi:10.1016/S0024-4937(03)00017-3.

Saul, J., M. R. Kumar, and D. Sarkar (2000), Lithospheric and upper mantle structure of the Indian Shield, from teleseismic receiver functions, *Geophys. Res. Lett.*, *27*(16), 2357–2360.

Silva, J. B., and M. F. Pereira (2004), Transcurrent continental tectonics model for the Ossa-Morena Zone Neoproterozoic-Paleozoic evolution, SW Iberian Massif, Portugal, *Int. J. Earth Sci.*, *93*(5), 886–896, doi:10.1007/s00531-004-0424-5.

Simancas, J. F. et al. (2003), Crustal structure of the transpressional Variscan orogen of SW Iberia: SW Iberia deep seismic reflection profile (IBERSEIS), *Tectonics*, *22*(6), 1062, doi:10.1029/2002TC001479.

Snyder, D. B. (1991), Reflections from a relic Moho in Scotland?, in *Continental Lithosphere: Deep Seismic Reflections. Geodynamics Series; vol. 22*, edited by O. Reilly and F. Head-clew, pp. 307–313, American Geophysical Union.

Snyder, D. B., and A. Flack (1990), Caledonian Age Reflectiors within the Mantle Lithosphere North and west of Scotland, *Tectonics*, *9*(4), 903–922.

Sochacki, J., R. Kubichek, J. George, W. R. Fletcher, and S. Smithson (1987), Absorbing boundary conditions and surface waves., *Geophysics*, *52*(1), 60–71, doi:10.1190/1.1442241.

Steer, D. N., J. H. Knapp, and L. D. Brown (1998), Super-deep reflection profiling: exploring the continental mantle lid, *Tectonophysics*, *286*(1–4), 111–121, doi:10.1016/S0040-1951(97)00258-8.

Stern, T. A., S. A. Henrys, D. Okaya, J. N. Louie, M. K. Savage, S. Lamb, H. Sato, R. Sutherland, and T. Iwasaki (2014), A seismic reflection image for the base of a tectoni plate, *Nature*, *518*(7537), 85–88, doi:10.1038/nature14146.

Stracke, A. (2012), Earth's heterogeneous mantle: A product of convection-driven interaction between crust and mantle, *Chem. Geol.*, *330–331*, 274–299, doi:10.1016/j.chemgeo.2012.08.007.

Taylor, G., S. Rost, and G. Houseman (2016), Crustal imaging across the North Anatolian Fault Zone from the autocorrelation of ambient seismic noise, *Geophys. Res. Lett.*, *43*(6), 2502–2509, doi:10.1002/2016GL067715.

Thybo, H., and D. L. Anderson (2006), The heterogeneous mantle, *Tectonophysics*, *416*(1–2), 1–6, doi:10.1016/j.tecto.2005.12.002.

Thybo, H., and E. Perchuc (1997), The Seismic 8 Discontinuity and Partial Melting in

Continental Mantle, *Science (80-.).*, *275*(5306), 1626–1629, doi:10.1126/science.275.5306.1626.

Torne, M., M. Fernàndez, J. Vergés, C. Ayala, M. C. Salas, I. Jimenez-Munt, G. G. Buffett, and J. Díaz (2015), Crust and mantle lithospheric structure of the Iberian Peninsula deduced from potential field modeling and thermal analysis, *Tectonophysics*, *663*, 419–433, doi:10.1016/j.tecto.2015.06.003.

Villaseca, C., E. Ancochea, D. Orejana, and T. E. Jeffries (2010), Composition and evolution of the lithospheric mantle in central Spain: inferences from peridotite xenoliths from the Cenozoic Calatrava volcanic field, edited by M. Coltorti, H. Downes, M. Gregoire, and S. . O'Reilly, *Geol. Soc. London, Spec. Publ.*, *337*(1), 125–151, doi:10.1144/SP337.7.

Villaseca, C., D. Orejana, and E. A. Belousova (2012), Recycled metaigneous crustal sources for S- and I-type Variscan granitoids from the Spanish Central System batholith: Constraints from Hf isotope zircon composition, *Lithos*, *153*, 84–93, doi:10.1016/j.lithos.2012.03.024.

Villaseca, C., P. Castiñeiras, and D. Orejana (2015), Early Ordovician metabasites from the Spanish Central System: A remnant of intraplate HP rocks in the Central Iberian Zone, *Gondwana Res.*, *27*(1), 392–409, doi:10.1016/j.gr.2013.10.007.

Vissers, R. L. M., M. R. Drury, E. H. H. Strating, and D. van der Wal (1991), Shear zones in the upper mantle: A case study in an Alpine Iherzolite massif, *Geology*, *19*(10), 990, doi:10.1130/0091-7613(1991)019<0990:SZITUM>2.3.CO;2.

Vissers, R. L. M., M. R. Drury, E. H. Hoogerduijn Strating, C. J. Spiers, and D. van der Wal (1995), Mantle shear zones and their effect on lithosphere strength during continental breakup, *Tectonophysics*, *249*(3–4), 155–171, doi:10.1016/0040-1951(95)00033-J.

Wang, Q., L. Burlini, D. Mainprice, and Z. Xu (2009), Geochemistry, petrofabrics and seismic properties of eclogites from the Chinese Continental Scientific Drilling boreholes in the Sulu UHP terrane, eastern China, *Tectonophysics*, *475*(2), 251–266, doi:10.1016/j.tecto.2008.09.027.

Warner, M., and S. McGeary (1987), Seismic reflection coefficients from mantle fault zones, *Geophys. J. R. Astron. Soc.*, *89*(1), 223–229, doi:10.1111/j.1365-246X.1987.tb04412.x.

Warner, M., J. Morgan, P. Barton, P. Morgan, C. Price, and K. Jones (1996), Seismic reflections from the mantle represent relict subduction zones within the continental lithosphere, *Geology*, *24*(1), 39–42, doi:10.1130/0091-7613(1996)024<0039:SRFTMR>2.3.CO;2.

Wilson, M., and H. Downes (1991), Tertiary - quaternary extension-related alkaline magmatism in Western and central Europe, *J. Petrol.*, *32*(4), 811–849, doi:10.1093/petrology/32.4.811.

Worthington, J. R., B. R. Hacker, and G. Zandt (2013), Distinguishing eclogite from peridotite: EBSD-based calculations of seismic velocities, *Geophys. J. Int.*, *193*(1), 489–505, doi:10.1093/gji/ggt004.

Zahradník, J., P. O'Leary, and J. Sochacki (1994), Finite-difference schemes for elastic waves based on the integration approach, *GEOPHYSICS*, *59*(6), 928–937, doi:10.1190/1.1443652.

Zand, G., and G. E. Randall (1985), Observations of shear-coupled P waves, *Geophys. Res. Lett.*, *12*(9), 565–568.

Zeck, H. P., M. T. D. Wingate, and G. Pooley (2007), Ion microprobe U–Pb zircon geochronology of a late tectonic granitic–gabbroic rock complex within the Hercynian Iberian belt, *Geol. Mag.*, *144*(01), 157, doi:10.1017/S0016756806002652.

Zelt, C. A., and R. B. Smith (1992), Seismic traveltime inversion for 2-D crustal velocity structure, *Geophys. J. Int.*, *108*, 16–34.

Zhang, Z., and T. Lay (1993), Investigation of Upper Mantle Discontinuities Near Northwestern Pacific Subduction Zones Using Precursors To Ssh, *J. Geophys. Res. Earth*, *98*(B3), 4389–4405.

Ziberna, L., S. Klemme, and P. Nimis (2013), Garnet and spinel in fertile and depleted mantle: insights from thermodynamic modelling, *Contrib. to Mineral. Petrol.*, *166*(2), 411–421, doi:10.1007/s00410-013-0882-5.

Zucali, M., J. M. Benitez Perez, D. Chateigner, J. Gomez-Barreiro, L. Lutterotti, and B. Ouladdiaf (2014), Rheology of the lower crust: Quantitative Texture Analysis of High Pressure - High Temperature rocks from Alps and Iberian Variscan belt., , doi:10.5291/ILL-DATA.1-02-163.

Figure 1. Tectonic map of the Iberian Peninsula with the location of the profiles analyzed in this study. The colored triangles mark the positions of the receiver stations and the yellow stars indicate the shot positions of the ILIHA-DSS, IBERSEIS-WA and ALCUDIA-WA wide-angle experiment (red, green and blue profiles, respectively). The Calatrava Volcanic Province (CVP) is indicated by a black solid triangle. DB: Duero Basin; GB: Guadalquivir Basin; TB: Tajo Basin; IS: Iberian System.

Figure 2. Stacked image of the ALCUDIA-NI transect in two-way travel time (twtt), modified after *Martínez Poyatos et al.* [2012]. Red arrows point the sub-Moho reflectors. Green arrow depicts the lower crust-uppermost mantle tectonic wedge.

Figure 3. Selected shot gathers from the ALCUDIA-WA experiment: shot 1 (top), shot 4 (middle), and shot 5 (bottom) (locations along the transect in Figure 1). The data have been band-pass filtered (5–20 Hz, see text. Filter bounds after frequency analysis, Figure 4), corrected for a spherical divergence, and amplitudes have been trace normalized. The shot records are displayed with a reduction velocity of 8.0 km/s. Phases labeled in the figure indicate the reflection and refraction at the base of the crust (PmP and Pn, respectively), and sub-Moho reflections under study in this work (PM1P and PM2P).

Figure 4. Frequency content of the PM1P phase for shot gathers 1 (a) and 4 (b), and PM2P for shot gathers 4 (c) and 5 (d) of the ALCUDIA-WA experiment. All shot gathers are plotted at 8.0 km/s reduced time. Note that the dominant frequencies are lower than 20 Hz.

Figure 5. Comparison of the polarity of the PM1P and PM2P arrivals with the PmP arrival observed on the ALCUDIA-WA shot gathers. All shot gathers are band pass filtered (5-20 Hz) and plotted at 8.0 km/s reduced time. Single wiggles are obtained from the stacked traces that encompass the reflections (red dashed box). Gray band indicates the energy group of each analyzed phase with the arrows pointing to the first larger amplitude.

Figure 6. a) P-wave velocity model for the ALCUDIA-WA experiment resulting from the forward modeling. Reflectors are marked in yellow. Tectonic zones are indicated on the top of the velocity model, colored according to figure 1. OMZ: Ossa Morena Zone, CIZ: Central Iberian Zone, TB: Tajo Basin. Raytracing diagrams are plotted in the bottom panels on top of the P-wave velocity model to illustrate the sampled reflectors for shot gathers 1 (b), 4 (c) and 5 (d). Theoretical travel time branches predicted by the resulting P-wave velocity model are drawn on top of the reduced velocity shot gathers to illustrate their alignment with the observed phases (top panel).

Figure 7. P-wave velocity models and subcrustal arrival times for the ILIHA-DSS experiment resulting from the forward modeling: a) Line DA, b) Line BX, c) Line CF, and d) Line BE. Top panels: shot gathers* showing theoretical travel time arrivals predicted by the resulting P-wave velocity model (red dots) plotted on top of the subcrustal arrivals (blue dots) from Iliha DSS Group [1993] to illustrate their alignment with the observed phases. Bottom panels: Resulting P-wave velocity models obtained in this study. Reflectors are marked in yellow. Tectonic zones are indicated on the top of each velocity model, colored according to figure 1. SPZ: South Portuguese Zone, OMZ: Ossa Morena Zone, CIZ: Central Iberian Zone, DB: Duero Basin, GB:

Guadalquivir Basin, BS: Betic System, IS: Iberian System. *Shot record B1 (line BE) could not be recovered due to irreparable damage on the tape where it was stored.

Figure 8. Map projection of the obtained depth of the sampled upper mantle reflectors PM1P (left panel) and PM2P (right panel). The depth positions of the interfaces are labelled and colored according to the depth scale. The main tectonic units are indicated (black solid lines) as in figure 1. Dashed lines represent the location of the seismic lines ILIHA-DSS (red), IBERSEIS-WA (green) and ILIHA-WA (blue).

Figure 9. a) Tectonic map of the area indicating the position of the reference P-wave velocity model (b) (black solid line) and the shot positions used for the generation of the synthetic shot gathers (d). The position of the IBERSEIS-WA Transect B and ALCUDIA-WA is also indicated as a green and blue line, respectively, as well as the shot position as yellow stars. b) Top panel: Reference P-wave velocity model for the south Iberian lithosphere created from the P-wave velocity distribution of the IBERSEIS-WA for the SPZ and OMZ, and from the ALCUDIA-WA for the CIZ. Two ~15 and ~2 km thick small-scale heterogeneity zones are included at the depth where the PM1P reflection is modeled and at the base of the crust, respectively. Velocity fluctuations are randomly distributed following a 2.7 fractal dimension with velocity variations in the range ±0.1 km/s from the reference P-wave velocity model (bottom panel) (see text for detailed explanation). c) Field data registered by the IBERSEIS-WA Transect B and ALCUDIA-WA experiments that recorded sub-Moho reflectors and (d) corresponding synthetic acoustic full wave-field seismograms generated using the velocity model on b). Shot positions are labeled on a) and b). Shot gathers are plotted at a reduced velocity of 8.0 km/s. Interpreted primary phases are labeled in both real and synthetic datasets. Red segments, on both field (c) and synthetic (d) shot gathers, indicate the arrival times of the PM_1P and PM_2P calculated from the P-wave velocity model.

Experiment	*Line*	*Line length*	*Station spacing*	*Shot spacing*	*Source size*
ILIHA-DSS	Line DA	~720 km	5-10 km	1 Offshore at the edge of the line	1000 kg of explosive
	Line BX	~680 km	5-10 km	2 Offshore at each edge of the line	1000 kg of explosive
	Line CF	~1220 km	5-10 km	1 Offshore at the edge of the line	1000 kg of explosive
	Line BE	~900 km	5-10 km	1 Offshore at the edge of the line	1000 kg of explosive
IBERSEIS-WA	Transect A	330 km	400 m	6 shots at ~60 km apart (3 northern ones failed)	From the edge to the center: 1000, 750 and 500 kg
	Transect B	300 km	150 m	6 shots at 60 km apart	From the edge to the center: 1000, 750 and 500 kg
ALCUDIA-WA	Line 1	~300 km	350-400 m	5 shots 70 km apart	1000 kg

Table 1. Data acquisition parameters for the wide-angle reflection/refraction experiments presented in this work.

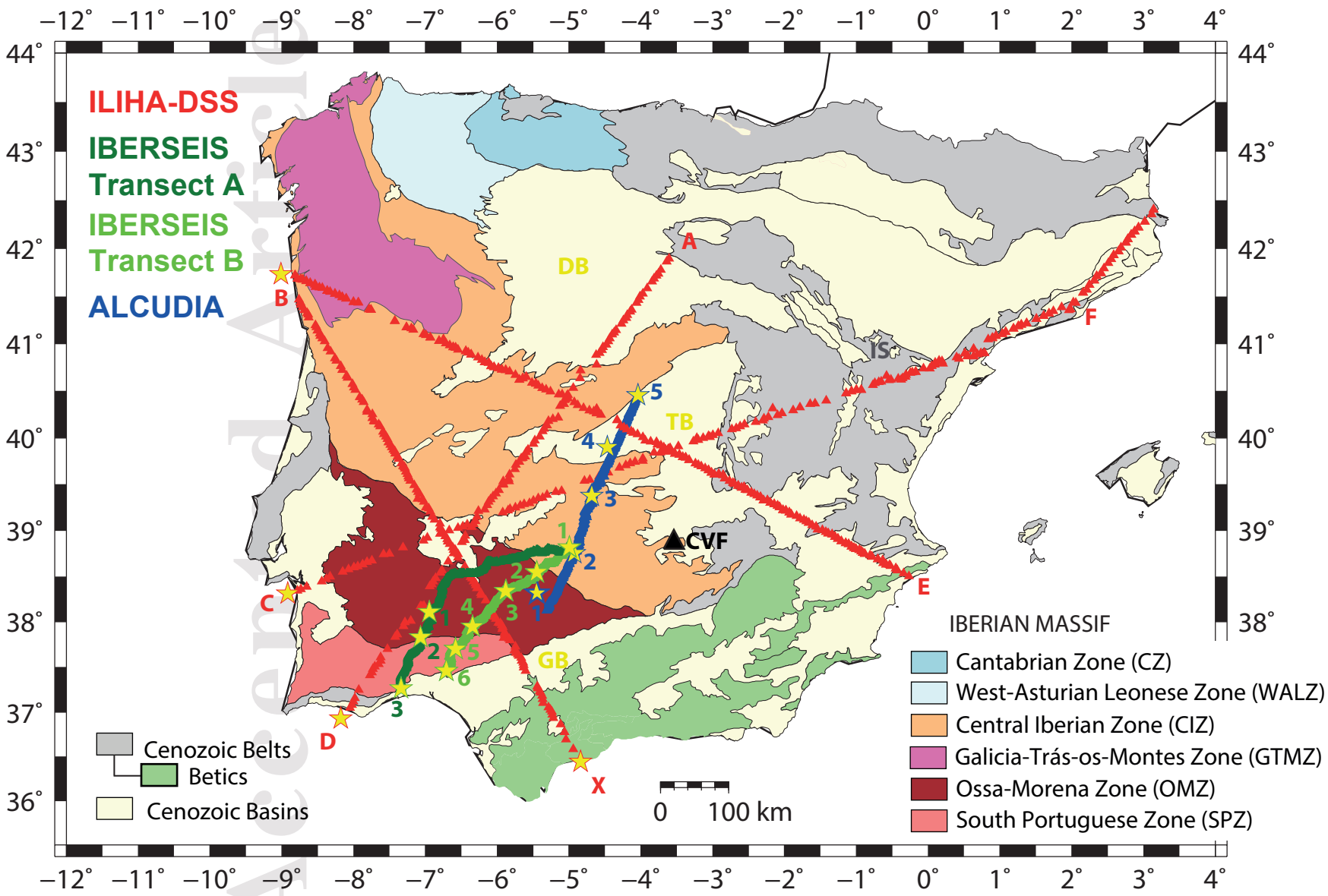

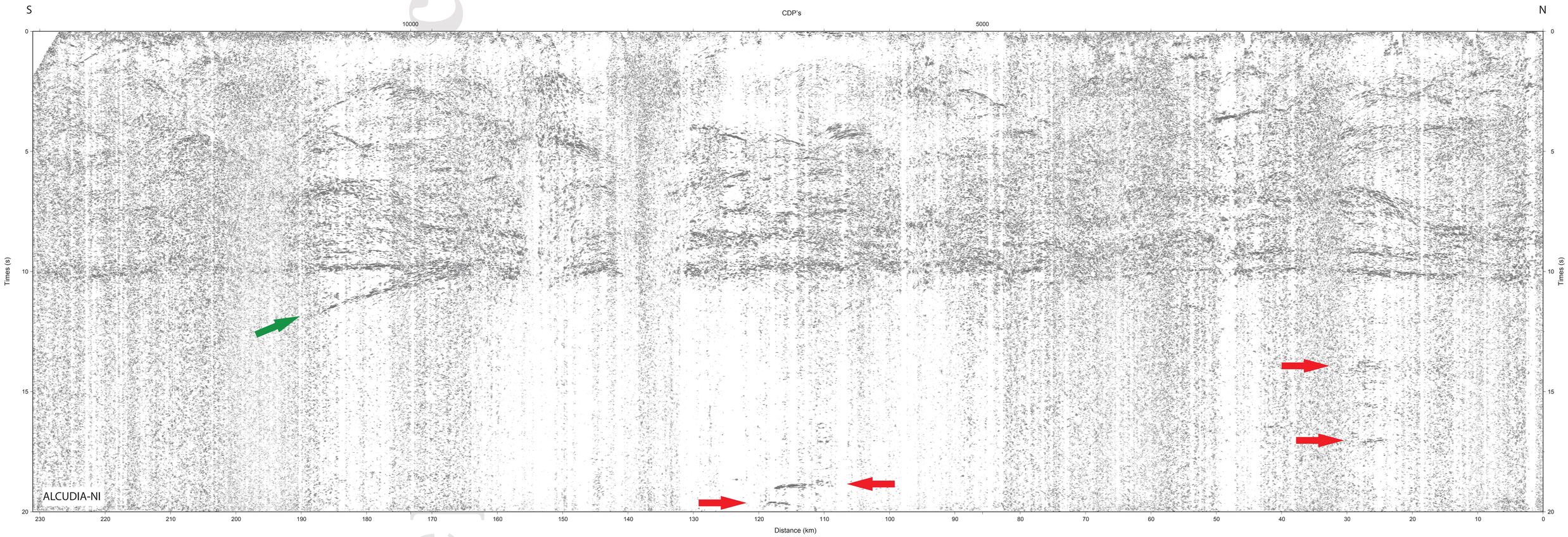

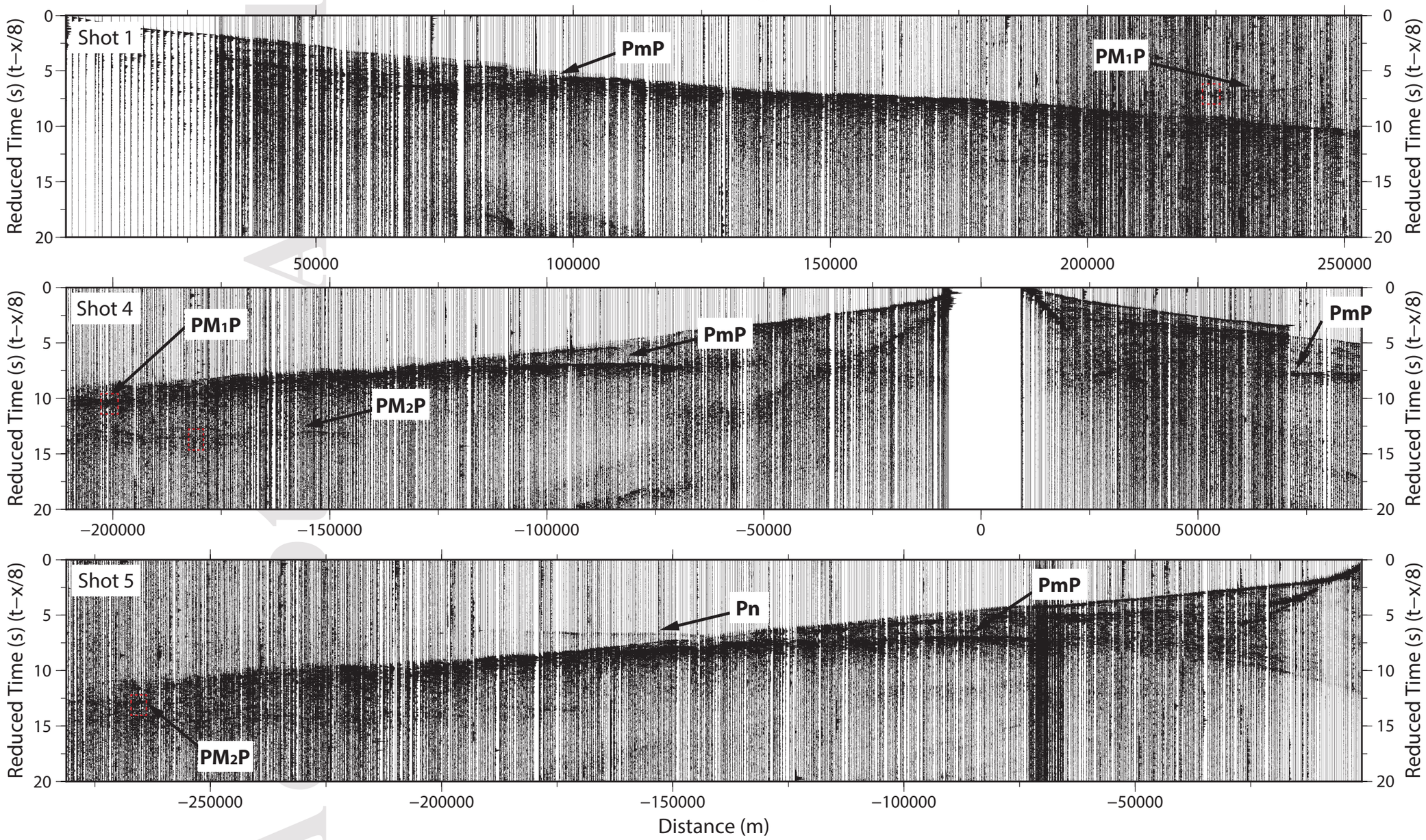

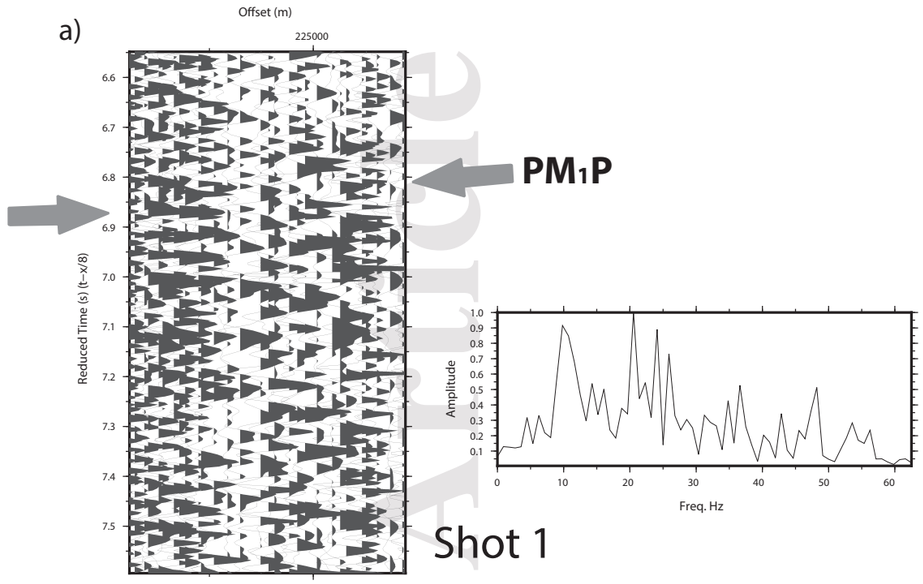

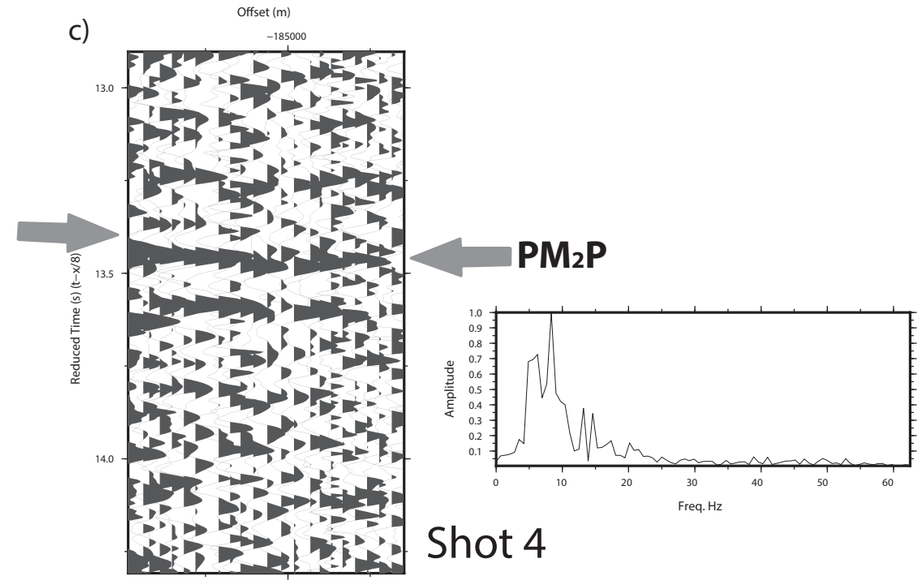

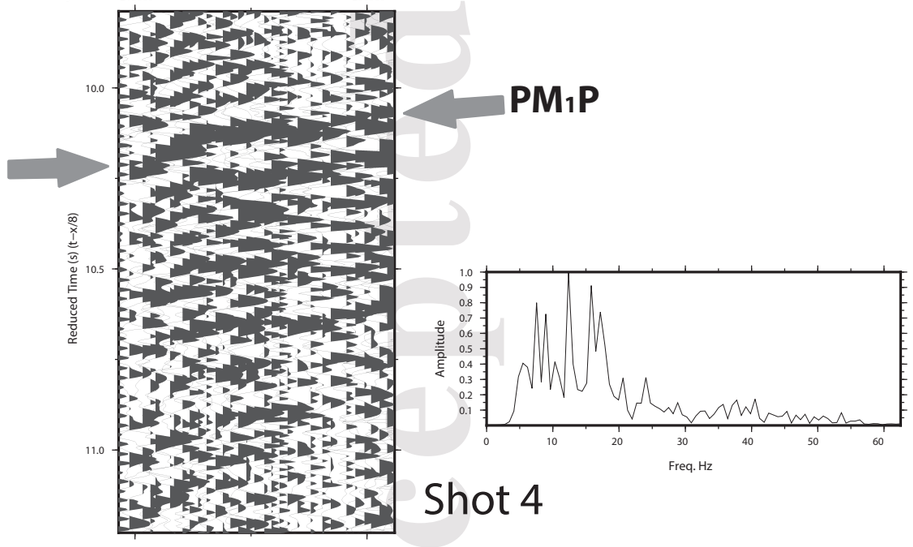

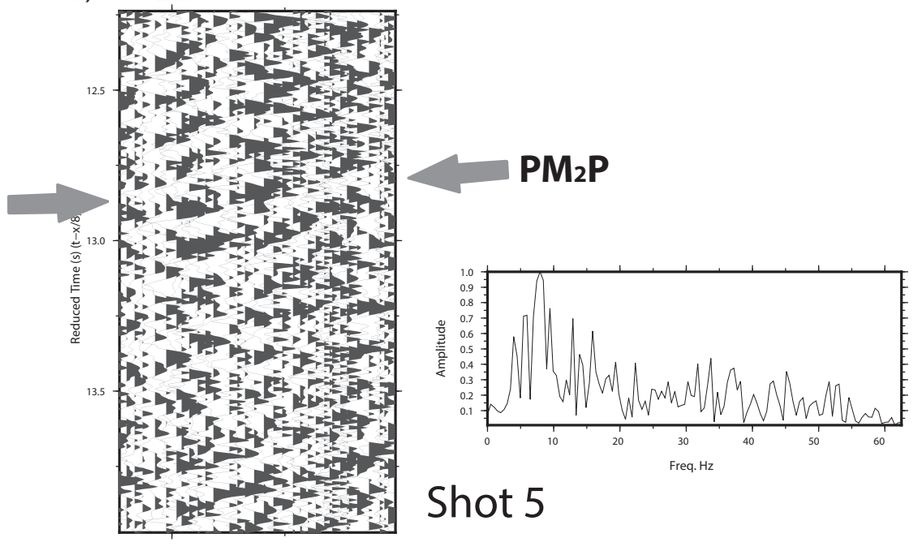

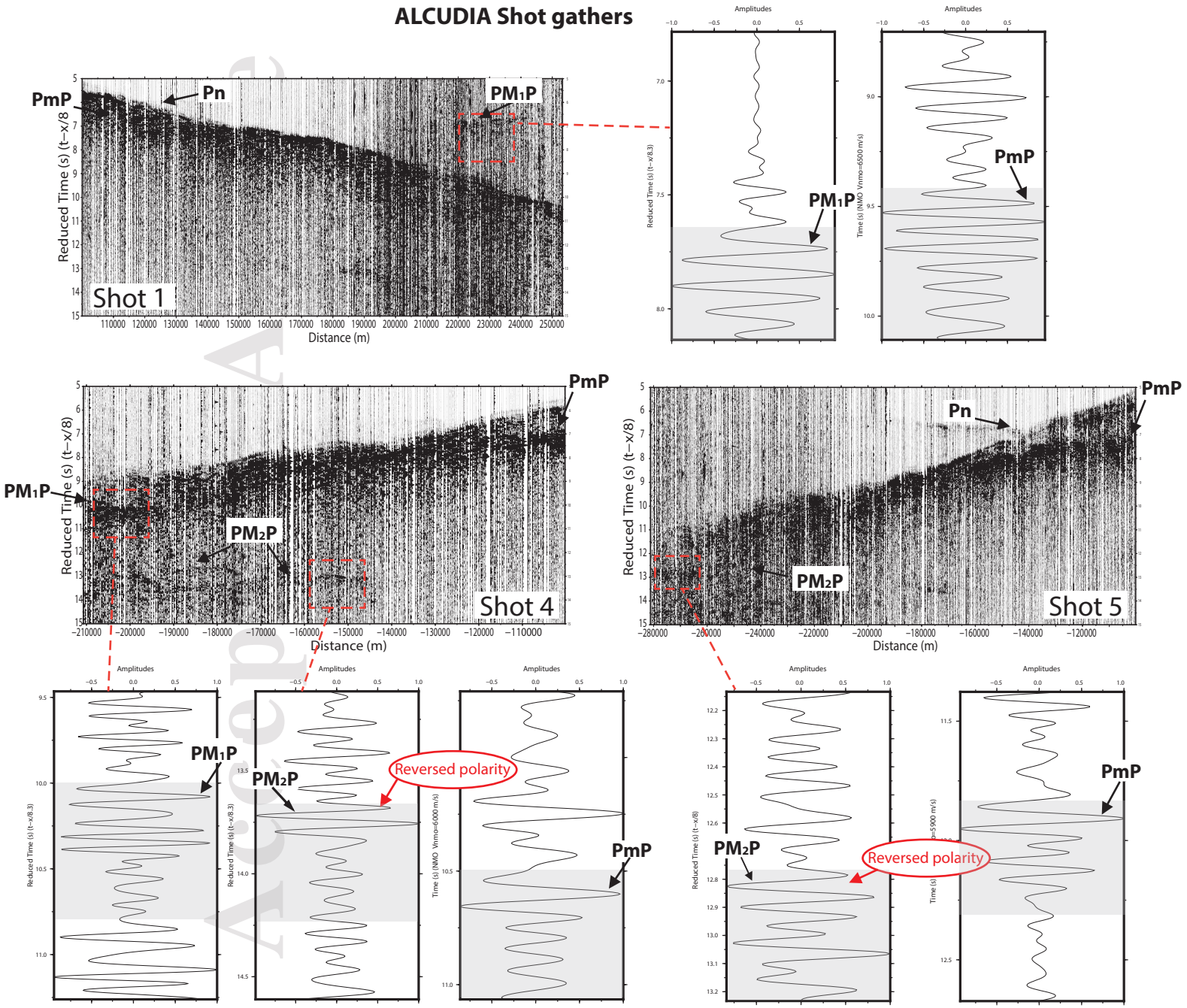

a)

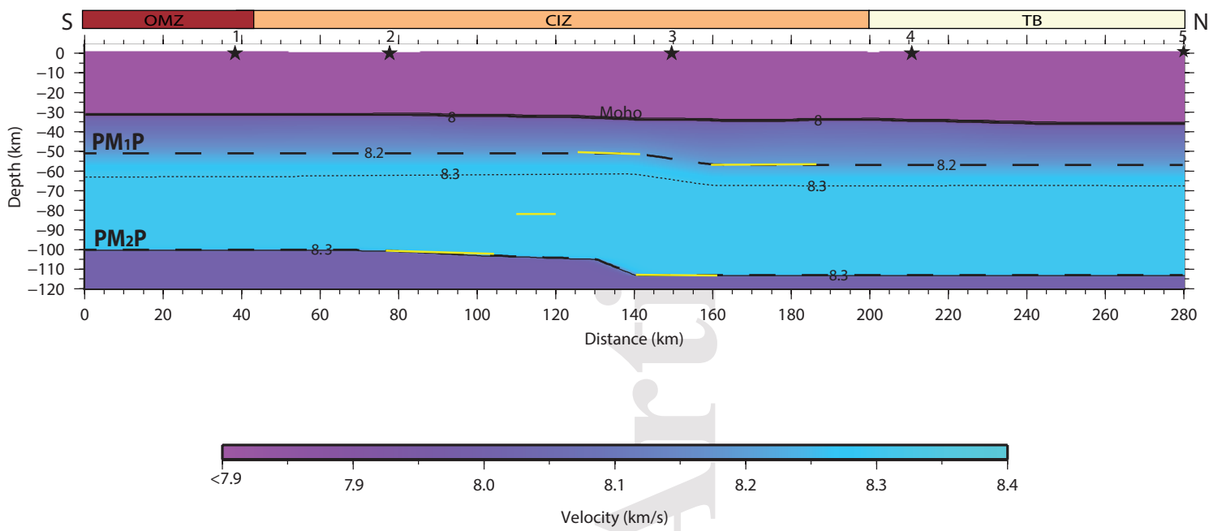

c)

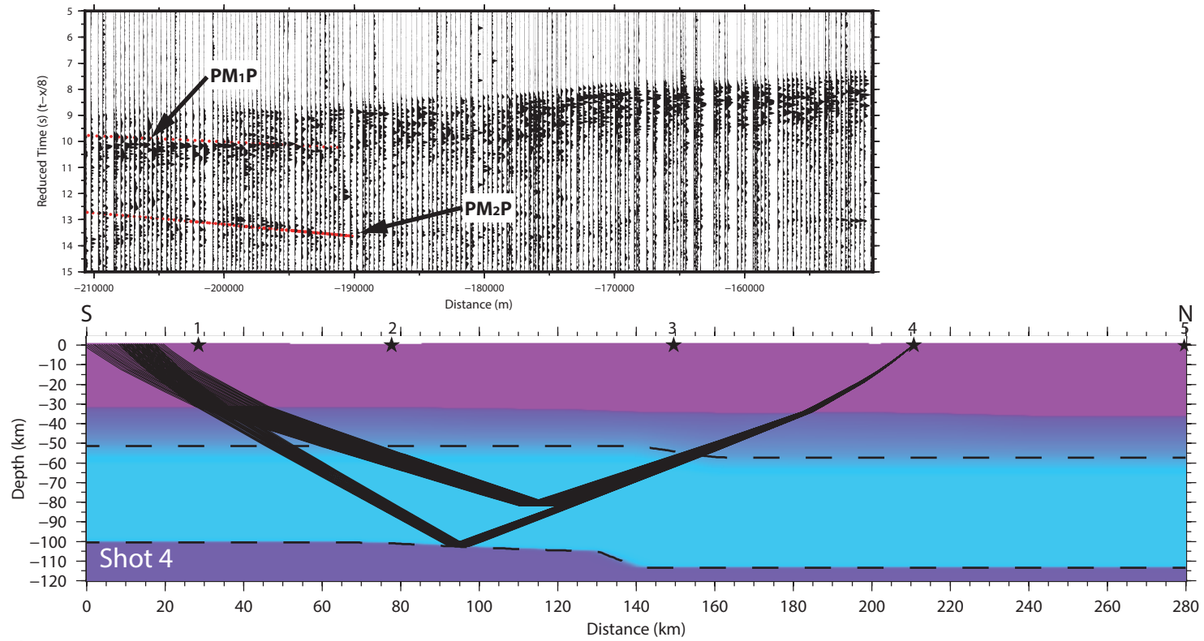

b)

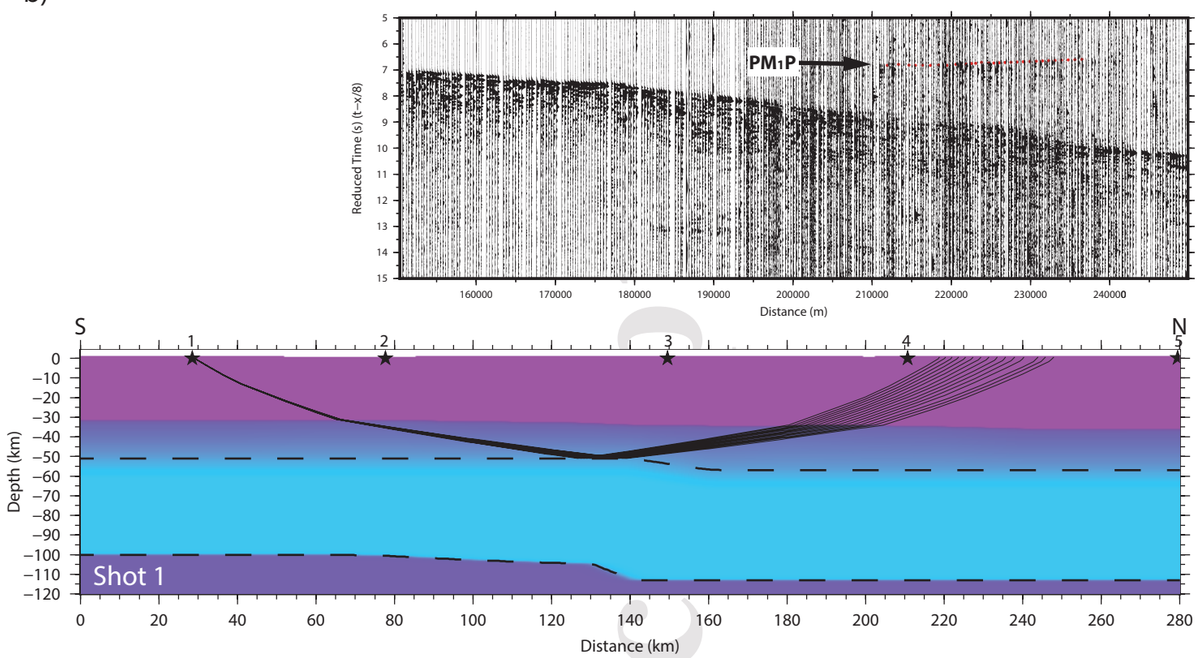

d)

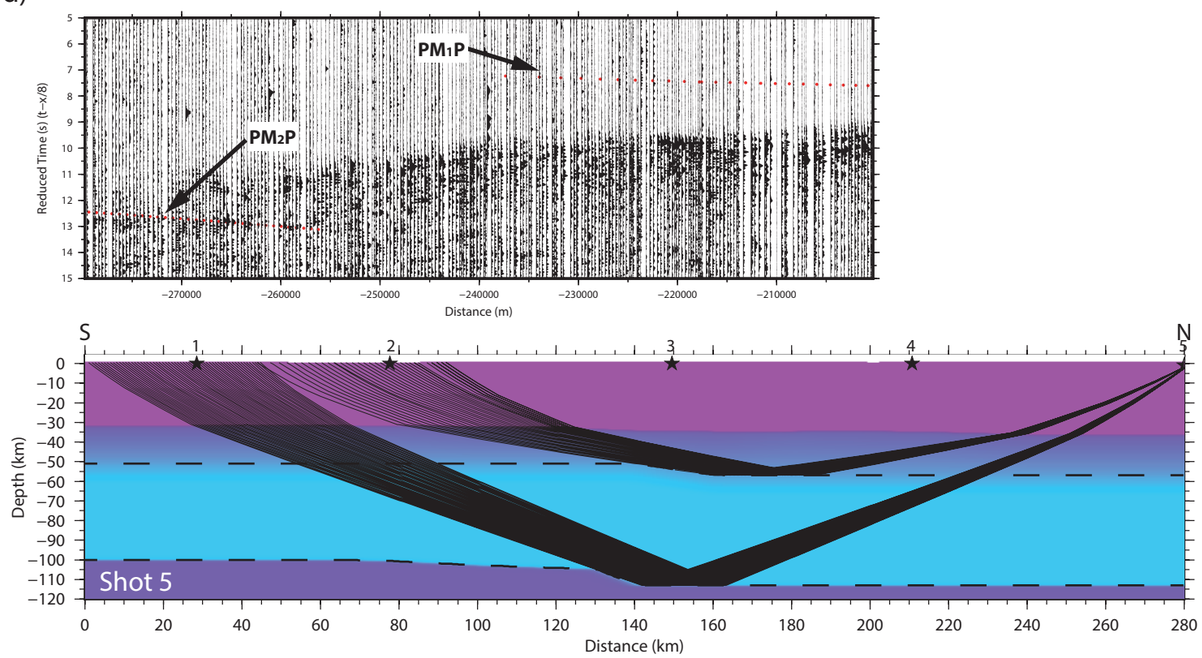

a)

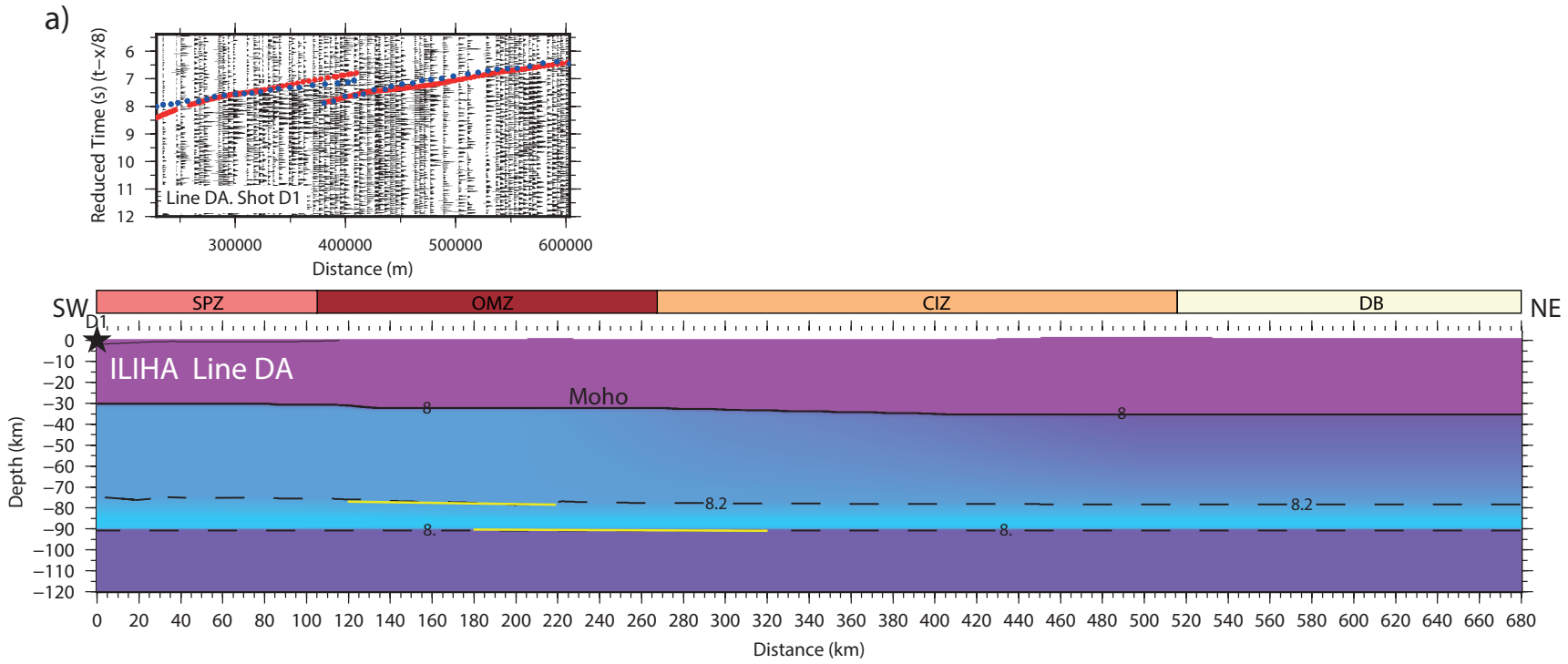

b)

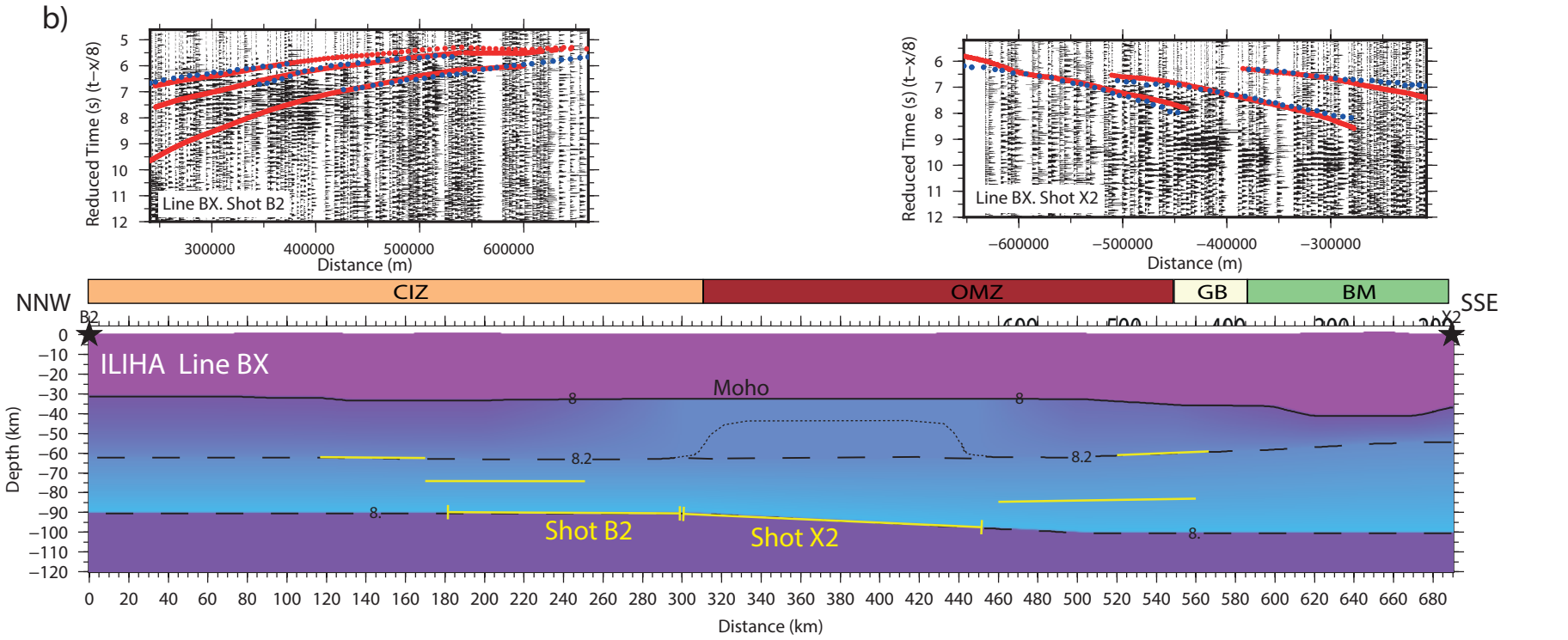

c)

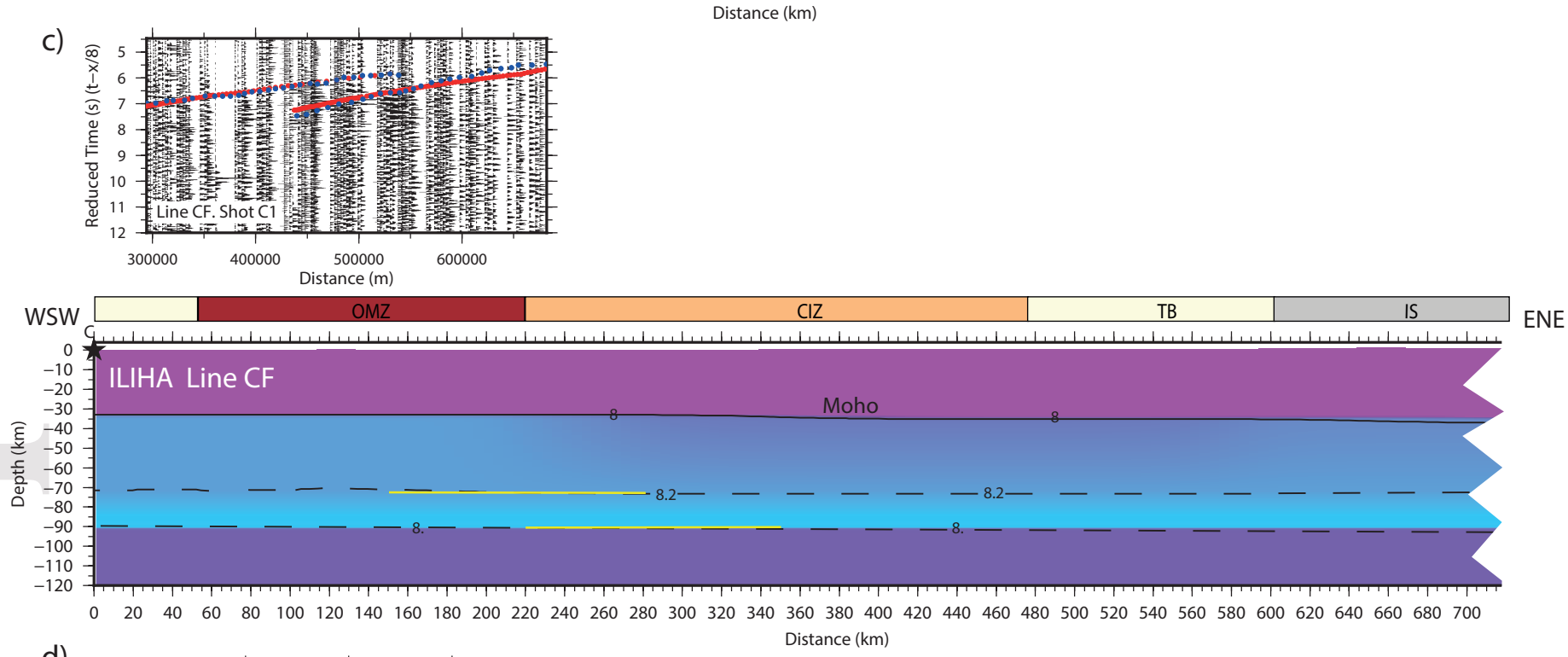

d)

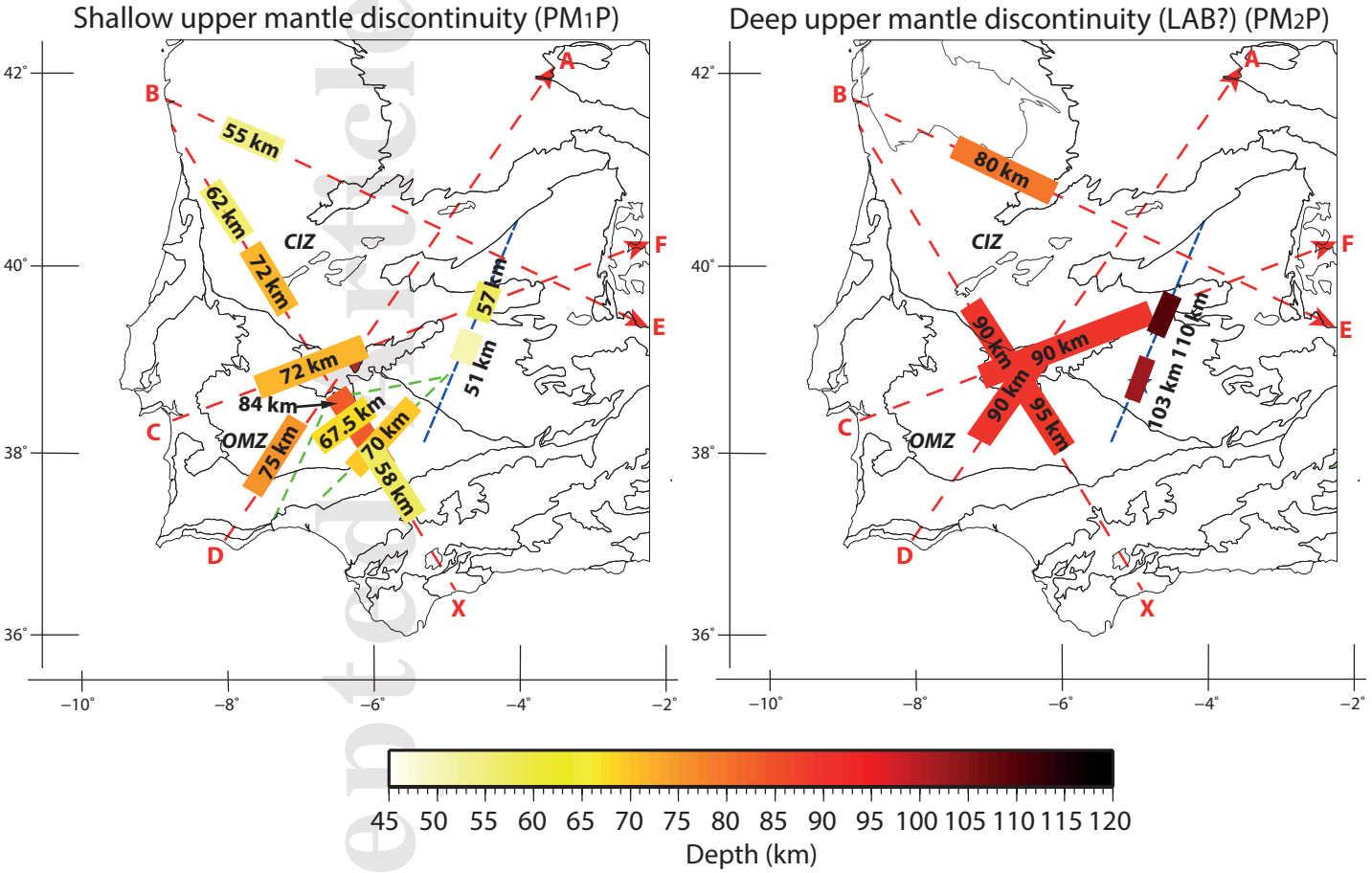

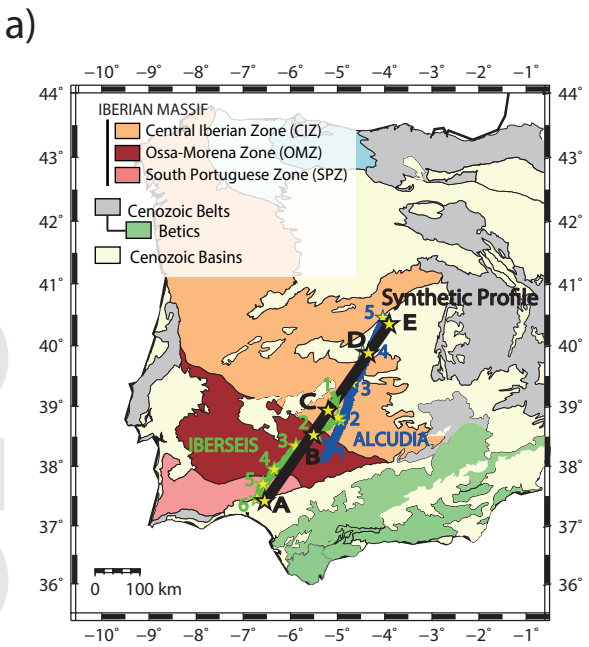

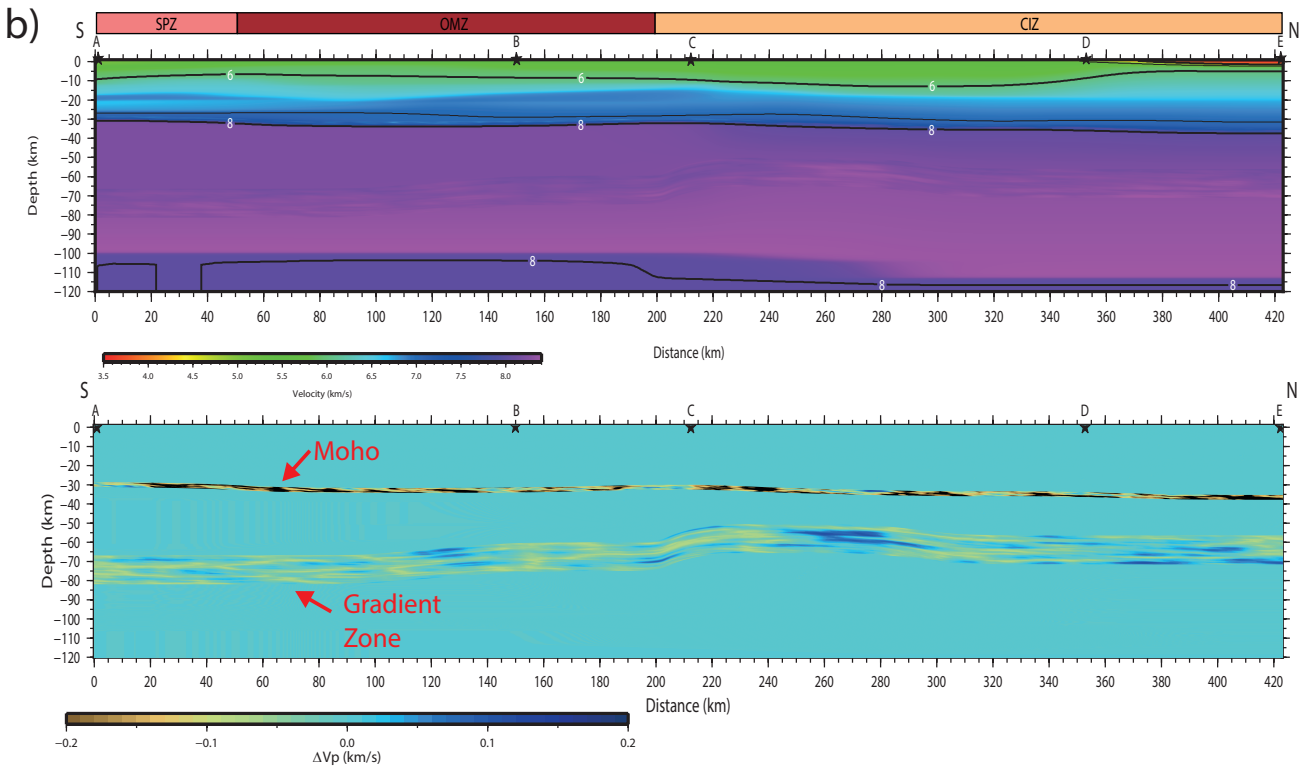

c) **FIELD DATA**

d) **ACOUSTIC FULL WAVE-FIELD SYNTHETIC SHOT**

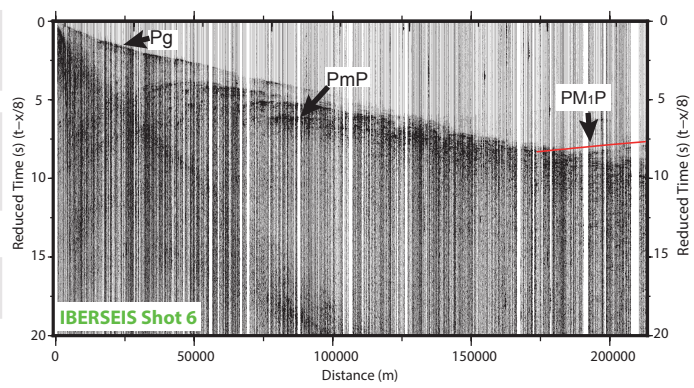

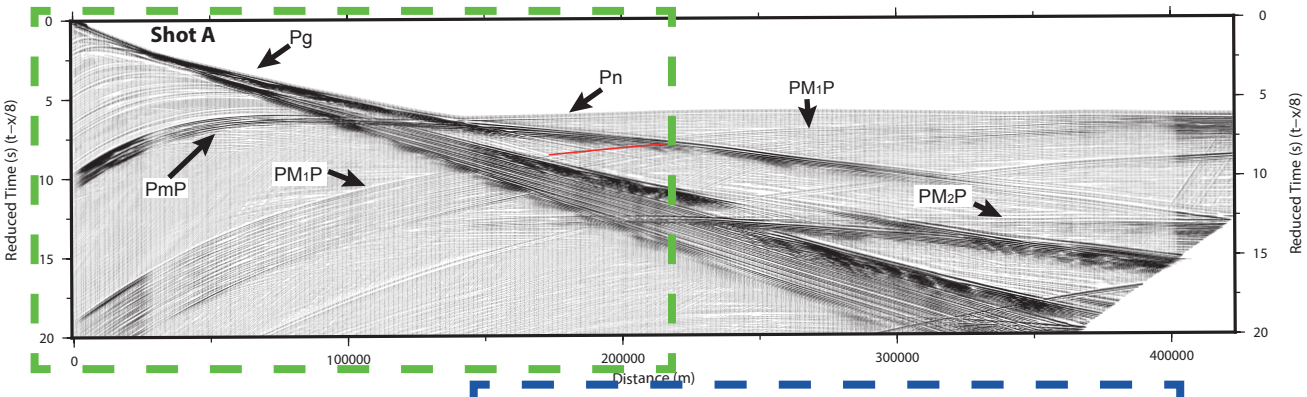

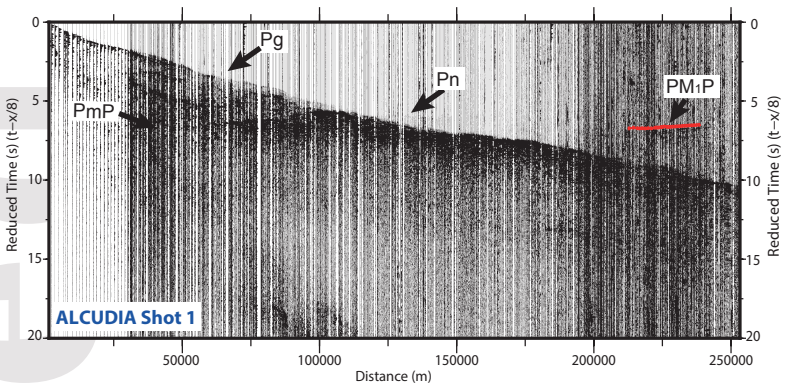

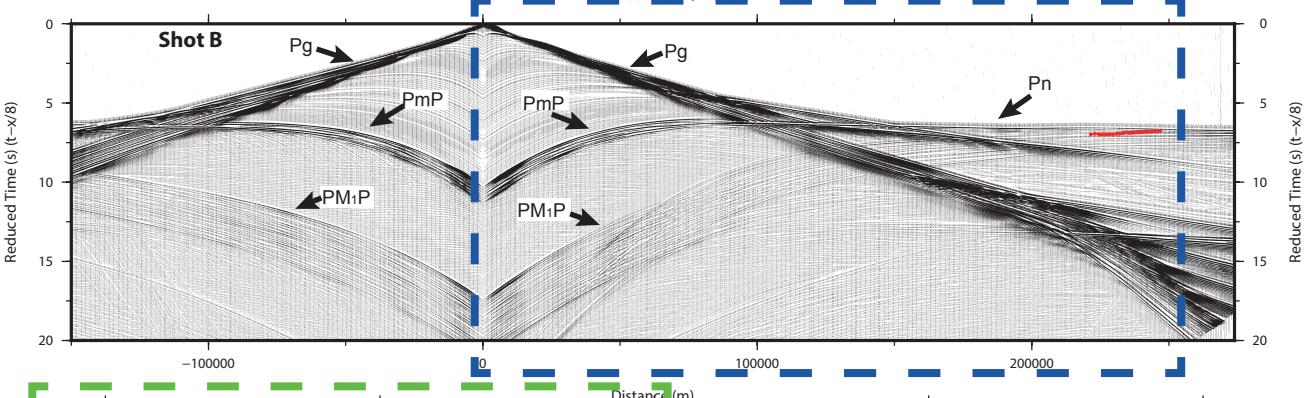

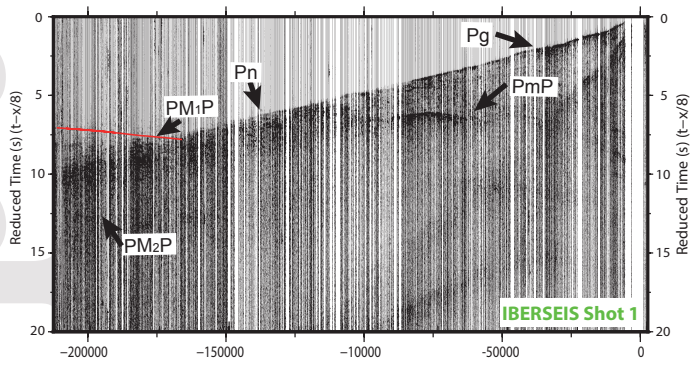

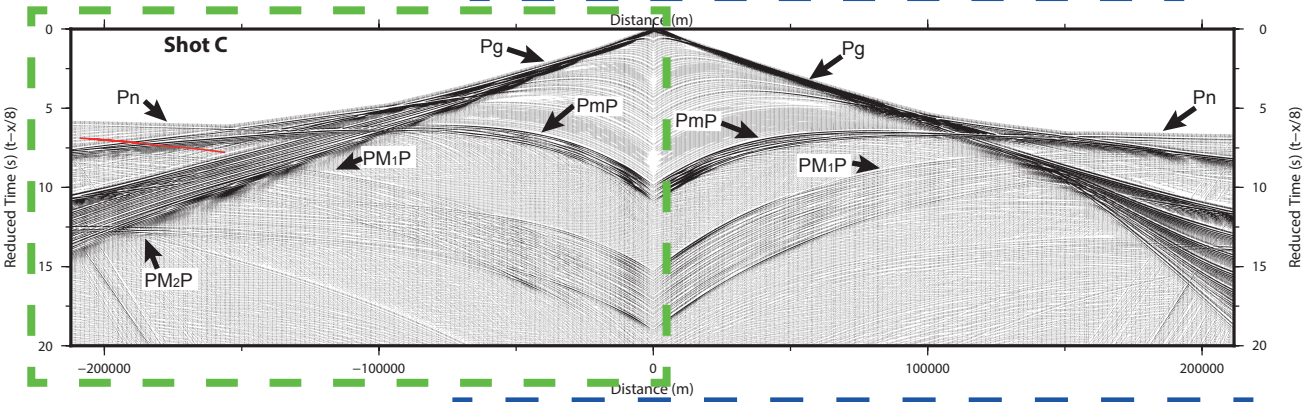

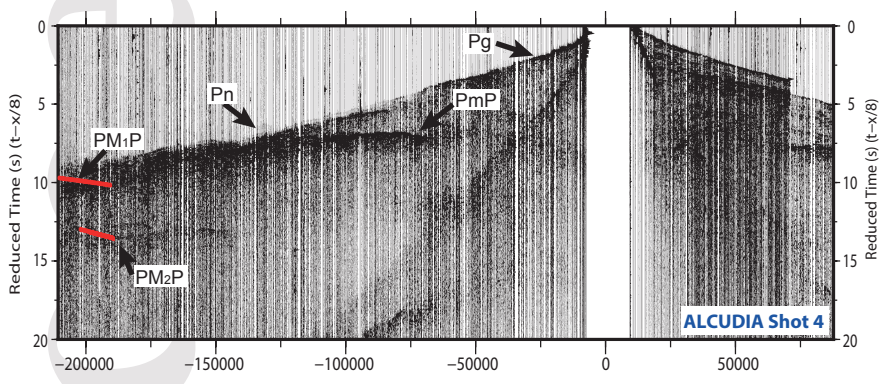

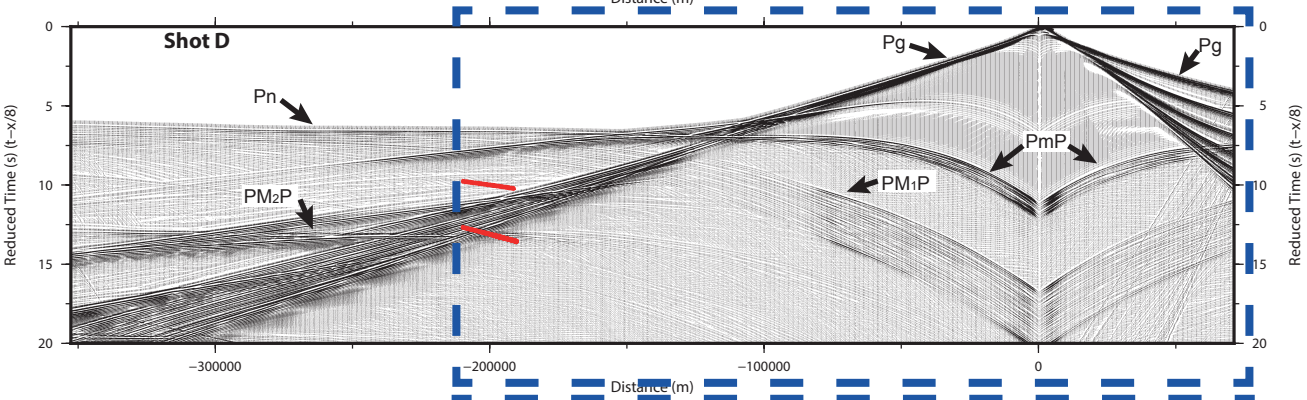

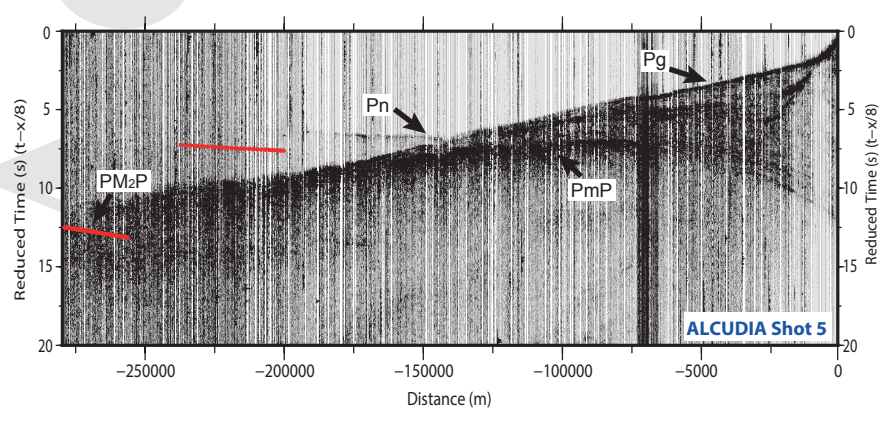

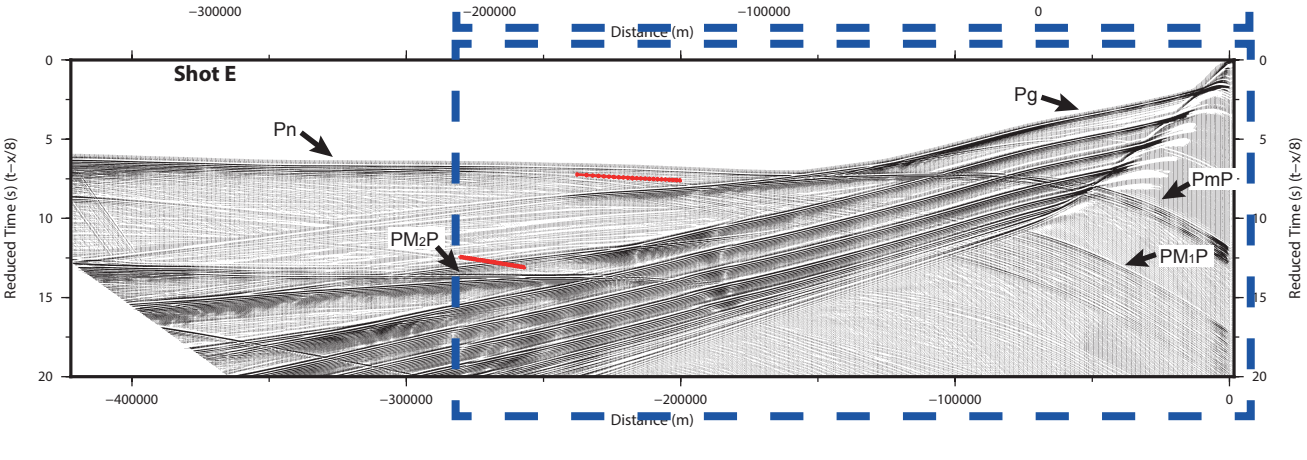

Supporting Information for:

Mapping and interpreting the Uppermost Mantle Reflectivity Beneath central and South-West Iberia

I. Palomeras[1], P. Ayarza[1], J. Andrés[2], A. M. Álvarez-Valero[1], J. Gómez-Barreiro[1], J. Díaz[2], J. Alcalde[2], R. Carbonell[2]

[1] Department of Geology, University of Salamanca, Salamanca, Spain

[2] Institute of Earth Sciences "Jaume Almera", ICTJA-CSIC, Barcelona, Spain

Corresponding author: Imma Palomeras (imma@usal.es)

Contents of this file

Figure S1

.

Introduction

This supporting information file contains figure S1. The figure shows the synthetic acoustic full wave-field seismograms generated using the velocity model resulting from the forward modeling with no heterogeneities included at Moho and depth of the uppermost mantle reflector. The images show how the arrival times are well recovered; however, the amplitudes and coda of the wavelet are not. Some heterogeneities need to be introduced at the considered depth in order to recover the wavelet characteristics by constructive interferences.

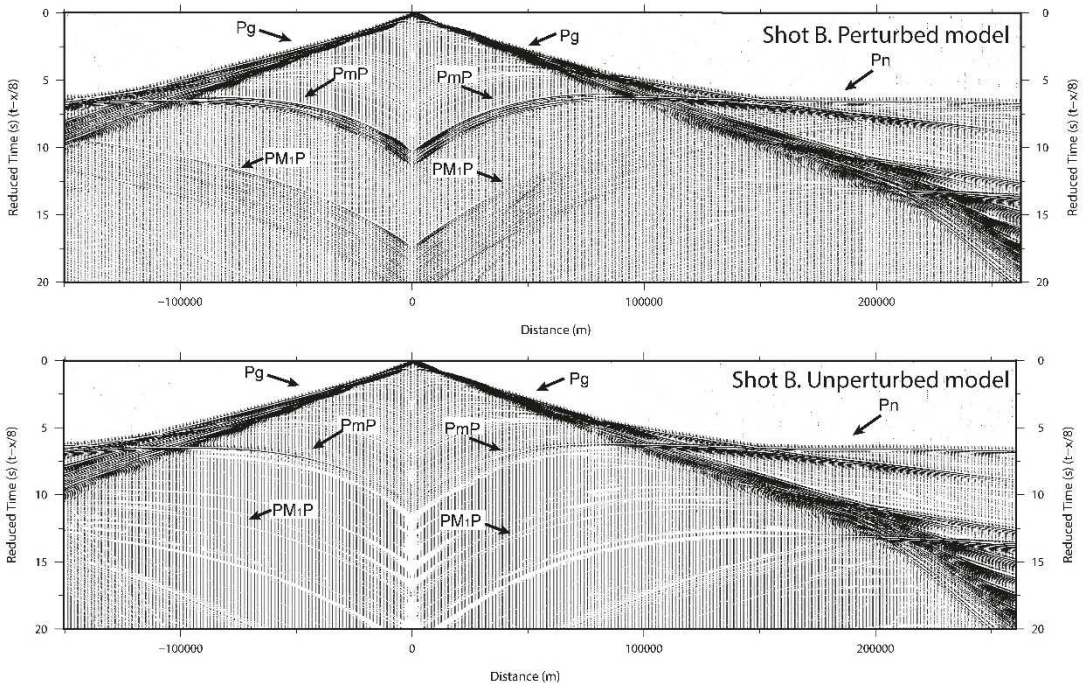

Figure S1: Acoustic full wave-field seismograms for shot B generated using the perturbed velocity model (Figure 9) (top panel) and the unperturbed velocity model (bottom pane). The high amplitude and ~1s coda of the PmP and PM_1P are recovered for the model with heterogeneities in the Moho and the uppermost mantle reflector.